NRIAG Journal of Astronomy and Geophysics (2012) 1, 119–140

National Research Institute of Astronomy and Geophysics

NRIAG Journal of Astronomy and Geophysics

www.elsevier.com/locate/nrjag

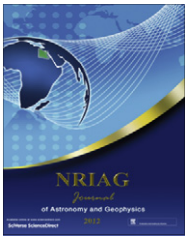

Seismic hazard studies in Egypt

Abuo El-Ela A. Mohamed [a,*], M. El-Hadidy [a,b], A. Deif [a,c], K. Abou Elenean [a,b]

[a] *National Research Institute of Astronomy and Geophysics, Egypt*
[b] *North Africa Group for Earthquake and Tsunami Studies, ICTP-OEA Net40, Italy*
[c] *Earthquake Monitoring Center, Sultan Qaboos University, Oman*

Received 22 May 2012; accepted 25 November 2012
Available online 18 February 2013

Abstract The study of earthquake activity and seismic hazard assessment of Egypt is very important due to the great and rapid spreading of large investments in national projects, especially the nuclear power plant that will be held in the northern part of Egypt. Although Egypt is characterized by low seismicity, it has experienced occurring of damaging earthquake effect through its history. The seismotectonic sitting of Egypt suggests that large earthquakes are possible particularly along the Gulf of Aqaba–Dead Sea transform, the Subduction zone along the Hellenic and Cyprean Arcs, and the Northern Red Sea triple junction point. In addition some inland significant sources at Aswan, Dahshour, and Cairo-Suez District should be considered. The seismic hazard for Egypt is calculated utilizing a probabilistic approach (for a grid of $0.5^\circ \times 0.5^\circ$) within a logic-tree framework. Alternative seismogenic models and ground motion scaling relationships are selected to account for the epistemic uncertainty. Seismic hazard values on rock were calculated to create contour maps for four ground motion spectral periods and for different return periods. In addition, the uniform hazard spectra for rock sites for different 25 periods, and the probabilistic hazard curves for Cairo, and Alexandria cities are graphed. The peak ground acceleration (PGA) values were found close to the Gulf of Aqaba and it was about 220 gal for 475 year return period. While the lowest (PGA) values were detected in the western part of the western desert and it is less than 25 gal.

Introduction

Egypt is located at the northeastern part of the African Continent (Fig. 1). With exception of the East African Rift which runs through Mozambique, Kenya, and Ethiopia, the African Continent is considered as a stable region. It collides with the Eurasian continent at the Mediterranean. The East African Rift branches in northern Ethiopia into two rifts along the Red Sea and along the Gulf of Aden. At the most northern part of the Red Sea Rift, the Red Sea Rift is branching into the Gulf of Suez and the Gulf of Aqaba. The Gulf of Aqaba

* Corresponding author. Tel.: +20 2 25560645.
E-mail address: abuoelela99@hotmail.com (A.E.-E.A. Mohamed).
Peer review under responsibility of National Research Institute of Astronomy and Geophysics.

2090-9977 © 2013 Production and hosting by Elsevier B.V. on behalf of National Research Institute of Astronomy and Geophysics.
http://dx.doi.org/10.1016/j.nrjag.2012.12.008

Fig. 1 Sketch showing the study area.

is known as a region of intensive crustal movement. The African content collides with Eurasian continent at the Mediterranean.

Egypt is located within zone of the plate boundaries, from, the southeastern side, the Red Sea Rift which is a zone of plate separation along which sea-floor spreading separates the African plate and Arabian plates apart, from the northeastern part, the Gulf of Aqaba–Dead Sea transform fault, which is a major left-lateral strike slip fault, which accommodates the motion between the Africa, Arabian and Eurasian plates, from the north Egypt is bounded by the subduction zone where, the African plate subduct beneath the Euraasian plate the at the Cyprean and Hellenic Arcs (Fig. 2).

Egypt is affected by earthquakes along the major tectonic structures of the plate margin as well as by those originating within the country itself (Fig. 3). Probabilistic Seismic Hazard Approach (PSHA) is performed, through different steps starting with, compiling a complete and homogenous earthquake catalog, delineation of a seismotectonic model that, this model is modified based on the works of Papaiouannou and Papazachos, 2000; El-Hadidy et al., 2008; Deif et al., 2011, using the proposed seismotectonic model and the seismotectonic model of Abou Elenean, 2010, different ground-motion prediction equations represent the different tectonic regimes were used to model the ground-motion in Egypt.

Both epistemic and aleatory uncertainties were considered during the hazard calculation, two seismotectonic source models and six attenuation models were used and weighted to account for the epistemic uncertainties, aleatory variability were minimized by giving priorities to the high quality data.

A revised earthquake catalog for Egypt and its surroundings during the period from 2200 BC to 2009 AD with magnitude equal or greater than three is compiled using information from several international and local seismic catalogs (Fig. 3).

The catalog was processed through different steps; removing repetitions, unifying magnitude scale the (moment magnitude), declustering the catalog to remove the dependent events (aftershocks, foreshocks, and earthquake swarms). This catalog also was tested for magnitude completeness. A great number of earthquakes faulting mechanisms were compiled from local and international sources, in order to be a powerful tool to indicate the present day stress regime of Egypt and its surroundings and to have a crucial role in delineating a representative seismotectonic model, using the collected focal mechanism, it is possible to define a representative mechanism for each seismic source.

Two seismotectonic source models were here considered, the first one consists of 77 seismic zones and reflects the author's point of view and is oriented toward capturing historical and instrumental seismicity, the identified active faults and the earthquake mechanism. The second is done by the work of Abou Elenean (2010). Based on the compiled earthquake catalog, sets of recurrence parameters (β, λ, and M_{max}) are estimated for each seismic zone. Suitable alternatives ground-motion scaling relationships for rock are used to produce 5% damped spectral acceleration values for different spectral

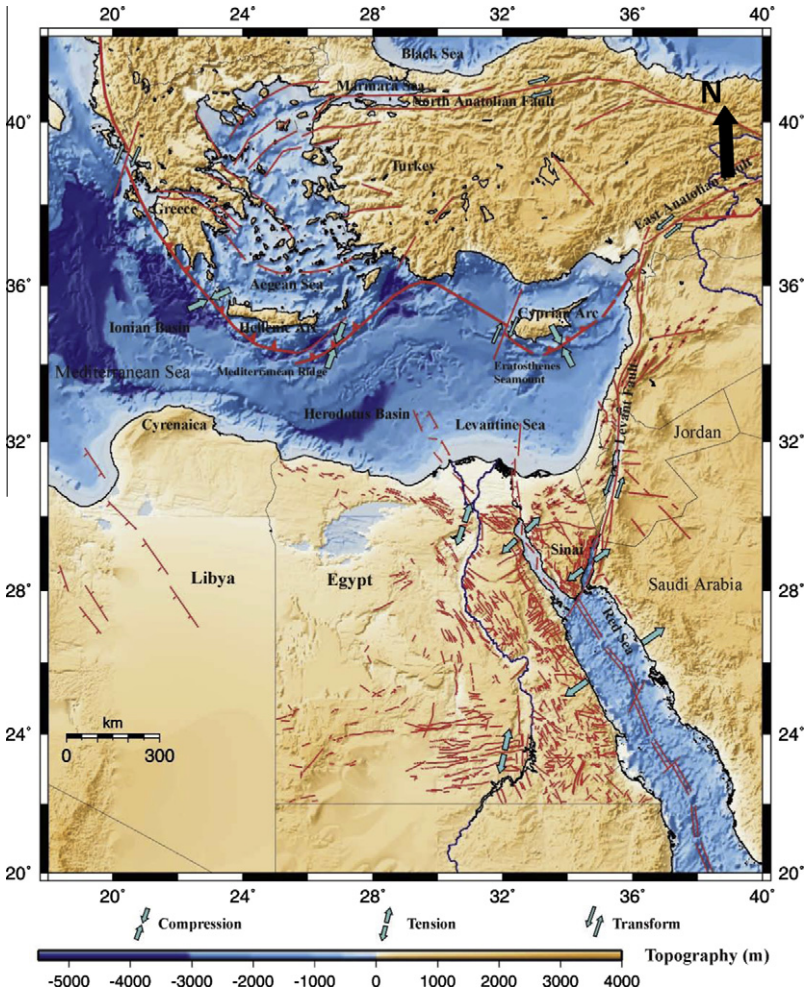

Fig. 2 Regional tectonic setting of the Eastern Mediterranean region (after Abou Elenean, 2004).

periods (PGA, 0.1, 0.2, 0.3, 1 s) for different return periods 475, 2475 years (equivalent to 10% and 2% probability of exceedance in 50 years respectively) in order to define approximate uniform hazard spectrum at 620 evenly distributed sites (Fig. 4). In addition, uniform hazard spectra for Cairo and Alexandria were calculated at 25 spectral periods and graphed.

Regional tectonics and seismicity

Egypt is located in the southeastern part of the Mediterranean Sea, and represents a subordinate part of the Eastern Mediterranean region. The Eastern Mediterranean Sea is a small ocean basin known by its unusual tectonic complexity. It is a relic of Mesozoic Neotetheys Ocean (Stampfli et al., 2001, Garfunkel, 2004), and includes a short segment of the convergence boundary between Africa and Eurasia. Subduction in this segment is along two very small arcs, the Hellenic and Cyprean arcs (Fig. 2).

Due to the complexity of the tectonics and deep structures of the Eastern Mediterranean area, the development of the Mediterranean area seems to be the result of crustal shortening due to the northward movement of the African Plate relative to the Eurasian Plate (Rabinowitz and Ryan (1970), McKenzie (1972), Comninakis and Papazachos (1972), Taymaz et al. (1990) Abou Elenean (1993)). Others however, suggested a varying mechanism for the tectonic process in this area. Hinz (1974) interpreted the data of seismic refraction and reflection surveys in the Ionian Sea as subsidence of an original continental crust.

Most of the seismicity and the seismic moments are concentrated and released within a seismogenic belt that stretches along the Dead Sea transform (DST), the Cyprean arc (CA), the Hellenic arc (HA), the Red Sea, and the Suez Rift (Salamon et al., 2003). The continuation of seismic activity is terminating north of the Gulf of Suez, showing that the area is still connected to the African Plate (Badawy and Horvath (1999), Salamon et al., (2003)).

The Aqaba–Dead Sea transform is a major left lateral strike slip fault that accommodates the relative motion between Africa and Arabia (Salamon et al., 1996). It extends for about 1000 km and connects a region of extension in the Northern Red Sea to the Taurus collision zone to the north.

This fault zone consists of en echelon faults with extensional jogs; with the largest such step over being the Dead Sea pull-apart basin. The main faults of this zone are trending N–S to NNE–SSW. They are found on the Sinai and Arabian deformed coastal areas as well as within the Gulf of Aqaba (Ben-Avraham, 1985). The deformation zone extends for a

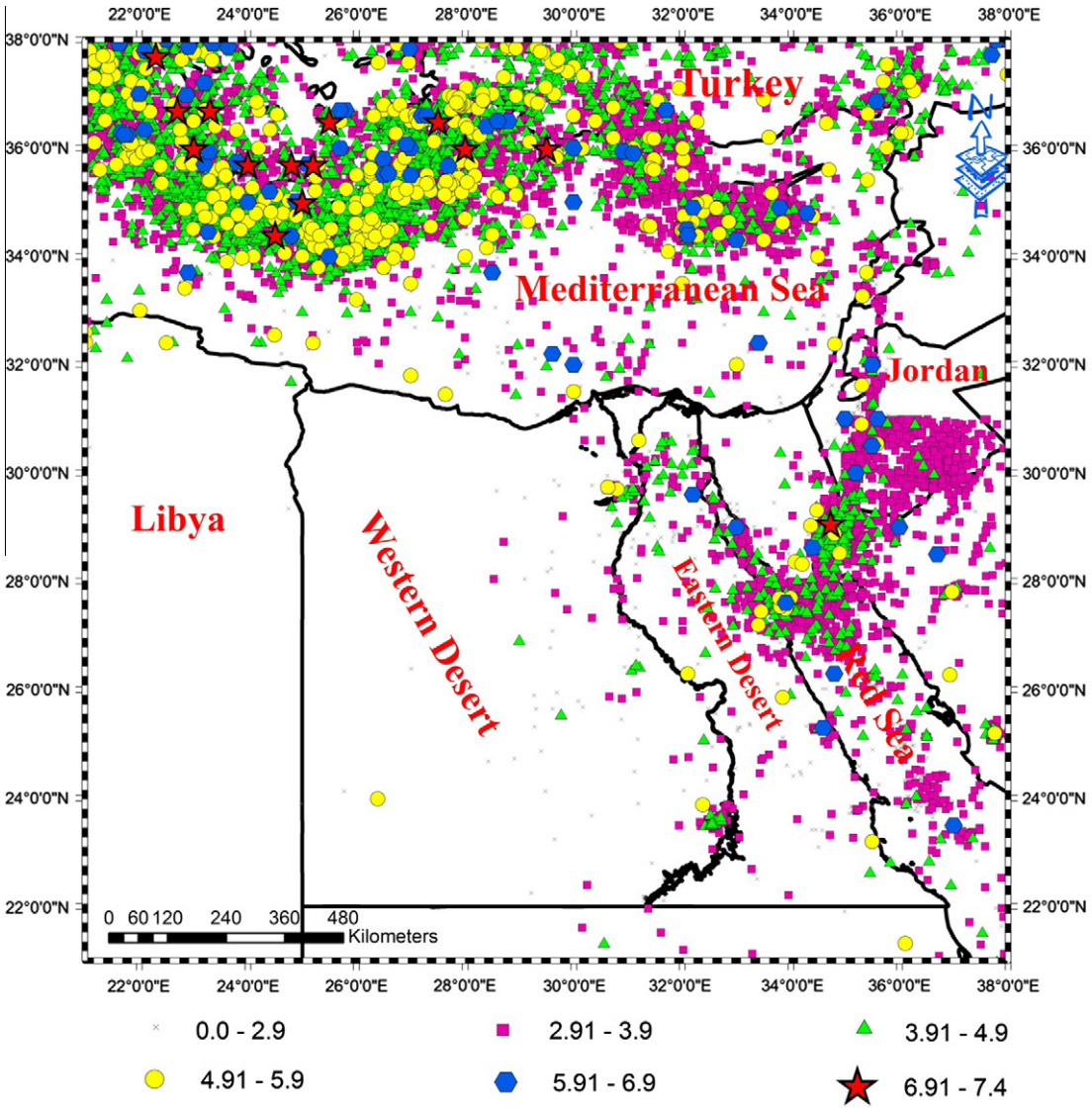

Fig. 3 Seismicity of Egypt based on the compiled earthquake catalog.

wider area along the Arabian side to about 60 km in the Midyan area but it is narrow at Wadi Araba to about 20 km. The 1800 m deep Gulf of Aqaba is considered to be a succession of NNE–SSW pull-apart basins dated to Late Miocene. The major faults of the Gulf of Aqaba as in (Fig. 5) are arranged en echelon, with transverse, probably normal faults at basin ends and interiors. The basins are therefore the product of extension at the step zones between the major left stepping strike slip faults (Ben-Avraham et al., 1979). This is consistent with the geological left-lateral offset along this plate boundary.

The Gulf of Aqaba region was affected by a number of earthquake swarms. The notable ones are those occurring in 1983, 1990 and 1993 (El-Isa et al., 1984; Alamri et al., 1991; Shamir and Shapira, 1994; Abdel-Fattah et al., 1997). The 1983 sequence consisted of 94 earthquake of magnitude $M_L > 3$ (largest magnitude $M_L = 5.2$), mostly confined to the Aqaba Basin. 1990–1991 swarm (largest magnitude $M_L = 4.3$) occurred mostly in the southern part of Aqaba Basin. The 1983–1991 activity was therefore, associated with the Aqaba–Aragonese fault step zone. On 22 November, 1995 an earthquake with magnitude ($M_w = 7.2$) hit the Gulf of Aqaba area. This earthquake is the largest recorded event in this area. This event is confined to the Aragones basin (Fig. 6).

Torlid and Hofstetter (1989), established a seismological network to study the seismicity of the Gulf of Aqaba–Dead Sea transform and found that most of the seismic activity is related to two main fault zones: the Jordan–Dead Sea rift and the Carmel and Faraa fault zones. Microearthquakes detected off Haifa, well outside the network, display a diffuse seismicity pattern, which suggests a continuation of the Camel–Faraa fault zone in the Mediterranean Sea.

The boundary between the African and the Anatolian-Aegean subplate is delineated by the Hellenic arc, the Pliny-Strabo trench, the Flornce Rise and Cyprus in the west, while in the East the boundary has been identified in the Herodotus basin or east of Cyprus (Aksu et al., 2005).

The Cyprean arc is a part of the plate boundary between Afro-Arabia and Eurasia in the Eastern Mediterranean. Seismic activity and gravity anomalies indicate that, a northward subduction of oceanic material related to the African Plate be-

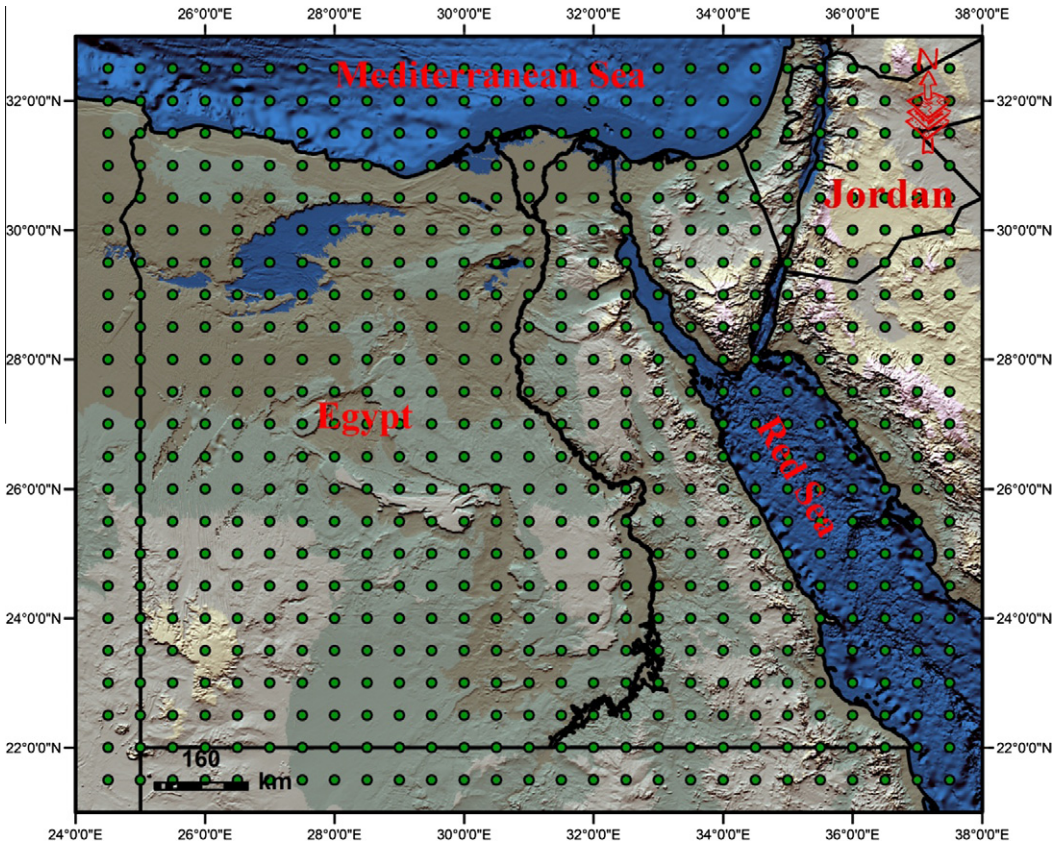

Fig. 4 The distribution of points for seismic hazard calculations.

neath the Turkish Plate is the mode of convergence along the western segment of the Cyprean arc (Ben-Avraham et al., 1988). Subduction is interrupted due to the collision of Eratosthenes seamount at the central segment of the Cyprean arc, which forms a zone of intense deformation (Giermann, 1969).

The zone of deformation spreads away and disappears in the eastern segment of the Cyprean arc. No signs of deformation have been found in this portion either in multichannel seismic reflection profiles, or in the bathymetry. The western portion of the Cyprean arc is severely deformed as indicated by disturbed bathymetry and seismic profiles. This zone of deformation has been suggested as a plate boundary (Wong et al. (1971), Lort et al. (1974), Ben-Avraham et al. (1976) and Ben-Avraham and Nur (1986)).

Seismic activity along this arc occurs in a wide seismogenic belt, which suggests that, the plate border is a zone of deformation instead of single line. The seismicity follows the accurate pattern of the arc. Most of the seismic activity took place in southern Cyprus, few of them occurred in the NW direction and very few in the NE of it. McKenzie (1970 and 1972). A continuous zone of seismicity can be traced from Cyprus into Zagros Mountain together with the sub-parallel seismic zone in Syria (Rotstein and Kafka, 1982). Papazachos and Comninakis (1978) suggested that the pattern of seismicity west of Cyprus is continuous and that a Benioff zone dipping to the north exists across the entire Eastern Mediterranean.

The Hellenic arc is generated by the active subduction of the oceanic lithosphere in the East Mediterranean with a NE–SW direction. It is a very small and bent arc with a slab subducting at a low angle (about 30°), which can be inferred from the fact that, the seismicity prevails at intermediate depths rather than deep. At the center of the Aegean Sea there is a series of volcanic systems almost parallel to the trench and forming the internal arc (Milos, Antimilos, Antiparos, Santorini, Kos, Yali, Nisiros, etc. (Le Pichon and Angelier, 1979).

The Red Sea occupies an elongated escarpment bounded depression between the uplifted Arabian and Nubian Shields. Stratigraphic and structural studies show that, the Red Sea and Gulf of Suez rifting began in Oligocene time and developed in Miocene (Fig. 2).

The shallow earthquake activity in the Hellenic arc is higher than the activity of the Cyprean arc. The activity of the Hellenic arc extends from Albania in the west to southwestern Turkey in the east. The activity is mostly seaward of the islands and all large events occur between the deepest part of the trench and islands. Few shocks lie as far as the Mediterranean ridge and the swell south of the deep basins. There is a low activity to the north of the arc, hence the southern part of the Aegean Sea is moving as a relatively rigid block compared with the surrounding zones (McKenzie, 1978).

Most events deeper than 100 km are located in the inner part of the arc (southern Aegean), while earthquakes shallower than 100 km are located along the sedimentary arc (Ionian, Crete, Rhodes) and its convex side (Eastern Mediterranean). The occurrence rate of intermediate foci earthquakes decreases from eastern to western side of the arc. A systematic increase in the focal depths from the outer part of the arc (Eastern Mediterranean) to the inner part (Aegean) is observed. That

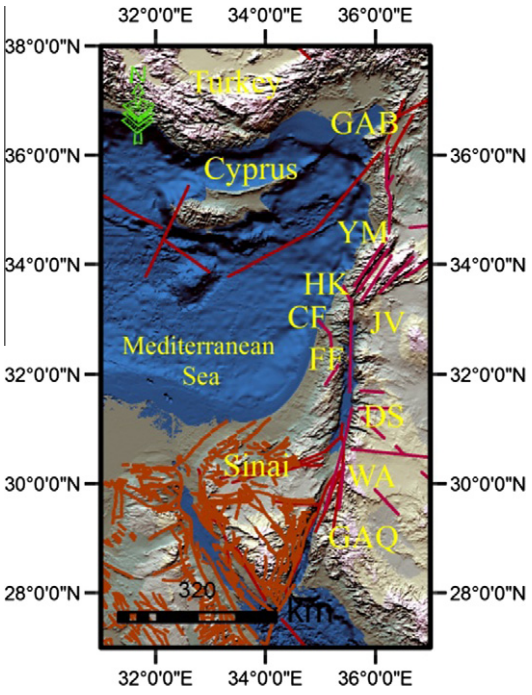

Fig. 5 Main tectonics of the Gulf of Aqaba–Dead Sea transform modified (After Garfunkel (1981), Klinger et al., (1999), Salamon et al., 2003). Abbreviations of geological elements and localities: CF, carmel fault; FF, fari fault; GAQ, Gulf of Aqaba; GS, Galilee Sea; HK, Hula and Kineret depressions; JV, Jordan valley fault; WA, Wadi-Araba; YM, Yammuneh fault.

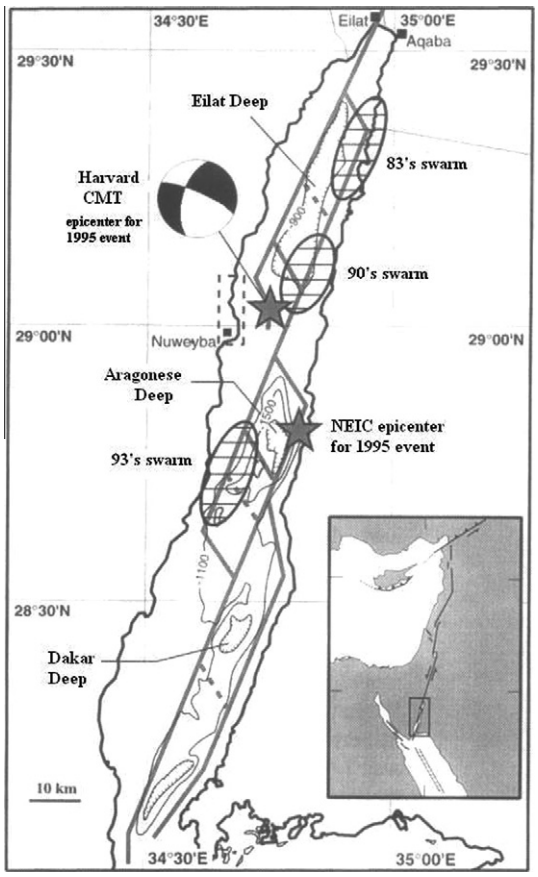

Fig. 6 Location map of the swarms of 1983, 1990, 1993 (after Abou Karaki et al. (1993); IPRG Seismological Bulletin (1996)).

is a well-defined Benioff zone, which dips from the convex to the concave side of the Hellenic arc. This zone has amphitheatrical shape, also the isodepth of 150 km roughly coincides with the line of volcanoes; Nysiros-Thera-Methana (Comninakis and Papazachos, 1980).

The northern province of the Red Sea is an active rift in the last stages of continental rifting, which began to undergo the transition to oceanic seafloor spreading. Based on morphological and structural features the Red Sea is divided into three distinct zones, each zone represents different stages of developments (Cochran and Martinez, 1988).

(1) Active-Seafloor Spreading Zone; This zone lies in the southern part of the Red Sea between latitudes 15° N and 20° N. It is characterized by a well-developed axial trough which developed through normal seafloor spreading during the last 5 Ma (Girdler and styles, 1978).
(2) Transition Zone; this zone is located in the central part of the Red Sea (20° N to 23° 20′ N) where the axial trough becomes discontinuous. It consists of a series of deeps alternating with shallow inter trough zones, the main trough is well developed.
(3) Late Stage Continental Rift Zone; this zone occurs north of the latitude 23° 20′ N and consists of a broad trough without a recognizable spreading center; the shelf areas are quite narrow. There are a number of small isolated deeps, (Cochran et al., 1986).

Fig. 3 shows that the seismic activity in the northern Red Sea is clustered at the entrance of the Gulf of Suez, the activity is continuous southward in the medial of the Red Sea. The cluster of the activity at this point may be due to the intersection of NW (Gulf of Suez–Red Sea) faults with the Aqaba trend and due to the plutonic activity. Few events are located in central Red Sea almost close to the transform faults crossing the rift axis.

The seismic activity extends to the north along the Suez Rift and includes the northern part of the Eastern Desert. This seismic trend is the major active trend inside the land of Egypt and extends toward Cairo and Alexandria toward northwest in the Mediterranean Sea. The activity of this trend is attributed to the Red Sea rifting as well as to several active faults, which have trends NNW parallel to the Red Sea–Gulf of Suez direction and its continuation toward East Mediterranean. Going south through the Red Sea, the seismic activity increases where the NE trending faults cross the spreading zone and its NW trending fault system, indicating that both Tertiary tectonic trends of the region are active.

Fairhead and Girdler (1970) reported the occurrence of large earthquake (m_b = 6) near the mouth of the Gulf of Suez at 27.62° N, 33.91° E on 31 March 1969 preceded by three foreshocks and followed by 17 aftershocks (m_b = 4.5–5.2) in the neighborhood of Shedwan Island.

After installation of the Hurghada seismic network 1994 at the northern part of the Red Sea, the seismicity data indicates two clear NW-SE trends in the Gulf of Suez region. The first

one extends about 125 km in length passing through the southern entrance of the Gulf of Suez with most of its activity around Gubal Island. Daggett et al. (1986) concluded that, this activity was attributed to the same source region of the important earthquake of 31 March 1969. The second trend is defined along the southwestern coast of Sinai Peninsula. The events of the two trends may be related to the bounding faults between the Precambrian outcrops of southern Sinai and the Gulf of Suez depression. Daggett et al. (1986) related the high rate of seismicity at the southern end of the Gulf of Suez to crustal movements between the Arabian and African Plates and Sinai subplate because of the opening of the Red Sea, extension in the Gulf of Suez and the left lateral strike-slip motion in the Gulf of Aqaba (Fig. 3). The epicenters of low to moderate seismic activity are clustered on the Gulf of Suez and its extension towards north in the Eastern Desert (Abou Elenean and Hussien, 2008).

The Gulf of Suez is bounded on the east by Sinai massive and on the west by the Red Sea hills of the Eastern Desert. The Gulf of Suez Rift consists mainly of three tectonic provinces that are separated by two accommodation zones. The northern accommodation zone trends ENE, while the southern zone trends WNW (Meshref, 1990). On either side of these fault zones the direction of tilt is reversed. The northern and southern tectonic provinces are characterized by a regional SW dip; on the other hand the central tectonic province is characterized by a regional NE dip. The southern edge of the Gulf of Suez is bordered by N–S faults which mark the transition between the shallow-water Suez basin and the deep (> 1 km) northern Red Sea Basin. The main direction of faulting along the entire Gulf is N330° (the Clysmic Trend parallel to the Gulf) and N10° (the Aqaba Trend). Both of these trends may be related to pre-existing structures (Robson, 1971). On June 12, 1983, an earthquake with magnitude about

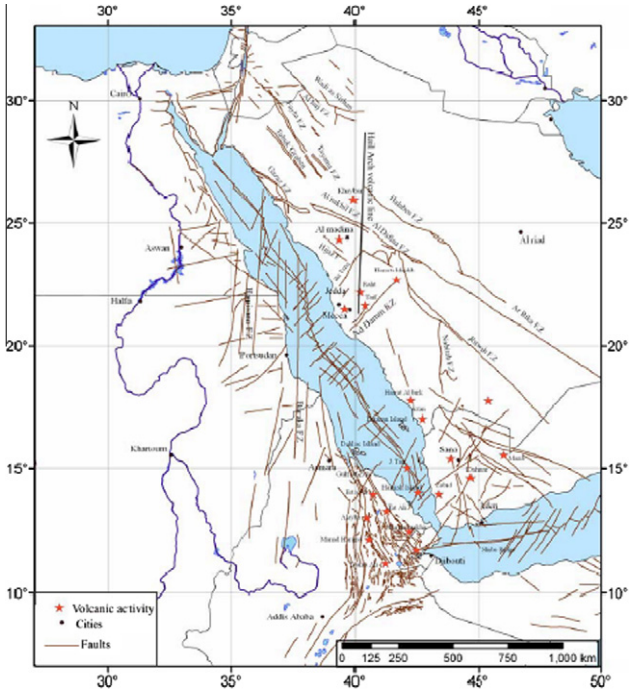

Fig. 7 Structural elements of the Red Sea and adjacent areas (after Babiker, 2009).

(m_b = 5.1), which was located in the central part of the Gulf of Suez, was felt in the region between Al-Aqaba and Beersheba, south Jordan as well as in Cairo Fig. 7.

The Seismic activity along the Eastern Desert is scattered, but there are some areas which produces earthquakes as Cairo-Suez shear zone, Beni-seuf zone, Abu Dabbab zone, south Abu Dabbab, and Barnis zone (Fig. 8). The moderate size earthquakes that occur in the Eastern Desert represent a source of seismic hazard on the people, who lives along the Nile valley and Nile delta. Although these earthquakes have moderate size, their impact is larger than the large earthquakes that occur in the Red Sea, Gulf of Suez, and Gulf of Aqaba.

Hosney et al., 2011 studied the seismicity and seismotectonics of Abou Dabbab area which lies at 24 km to the west of the western Red Sea coast between latitudes 24°N and 25°N. This study was done based upon the seismic data which were collected using a local seismic network through the period from 1, July 2004 to 20, August 2004. The data collected from this network had an important role in understanding the seismicity pattern, and the present day tectonic regime of Abou Dabbab area. Hosney et al., 2011 stated that according to the structural setting reported by the Egyptian Geological Survey an Mining Authority (EGSMA), 1996, the regional trends of major, minor faults and lineation are predominant by two major directions, the first one is the NNW–SSE which is parallel to the Red Sea coastal line, while the other set which is nearly perpendicular to the previous one (e.g., ENE–WSW).

Abd El-Tawb et al. (1993) studied the surface tectonic features of the area around Dahshour and Kom El-Hawa and they found a major N55°E trending normal fault at Kom El-Hawa (800 m length of surface trace with vertical displacement 40 cm) and a major E–W trending open fracture at Dahshour area (1200 m length). Also, Dahshour is experienced with historical earthquakes as those of 1847 with (M_F = 5.8) and 1895 with (M_F = 4.9). Abou Elenean (1997) considered the area of the epicenter of Dahshour Area (south west Cairo), the most catastrophic one in Egypt. Which took place on October, 12 1992 with M_L = 5.2.

Focal mechanisms of earthquakes occurring in Dahshour area indicate normal faulting with large strike slip component (Abou Elenean, 1997). The first nodal plane is trending nearly E–W, showing coincides with the surface lineaments, as appeared directly after the occurrence of 1992 earthquake and the general tectonic of the area.

Abou Elenean (2003) studied the seismicity and stress regime in Aswan area, he concluded his results as the following; the seismic activity is clustered in definite zones along specific trends. Few shocks are located far from the known faults, which may be due to location errors (Fig. 9).

(1) The activity is concentrated along the E–W trending Kalabsha fault and its extension towards east in consistence with surface trace of the fault (Fig. 10).
(2) Cluster of seismic activity along faults trending N–S is observed at the southern ends of both Khur El Ramla and Kurkur faults. Low activity observed in N–S direction along Abu-Dirwa fault and at the intersection of Gabal El-Baraq and Syial faults (Fig. 10).
(3) A cluster of small earthquakes located in the middle part of Nasser Lake following E–W direction. Also, there is a cluster of smaller events at the northern tip of Dabud

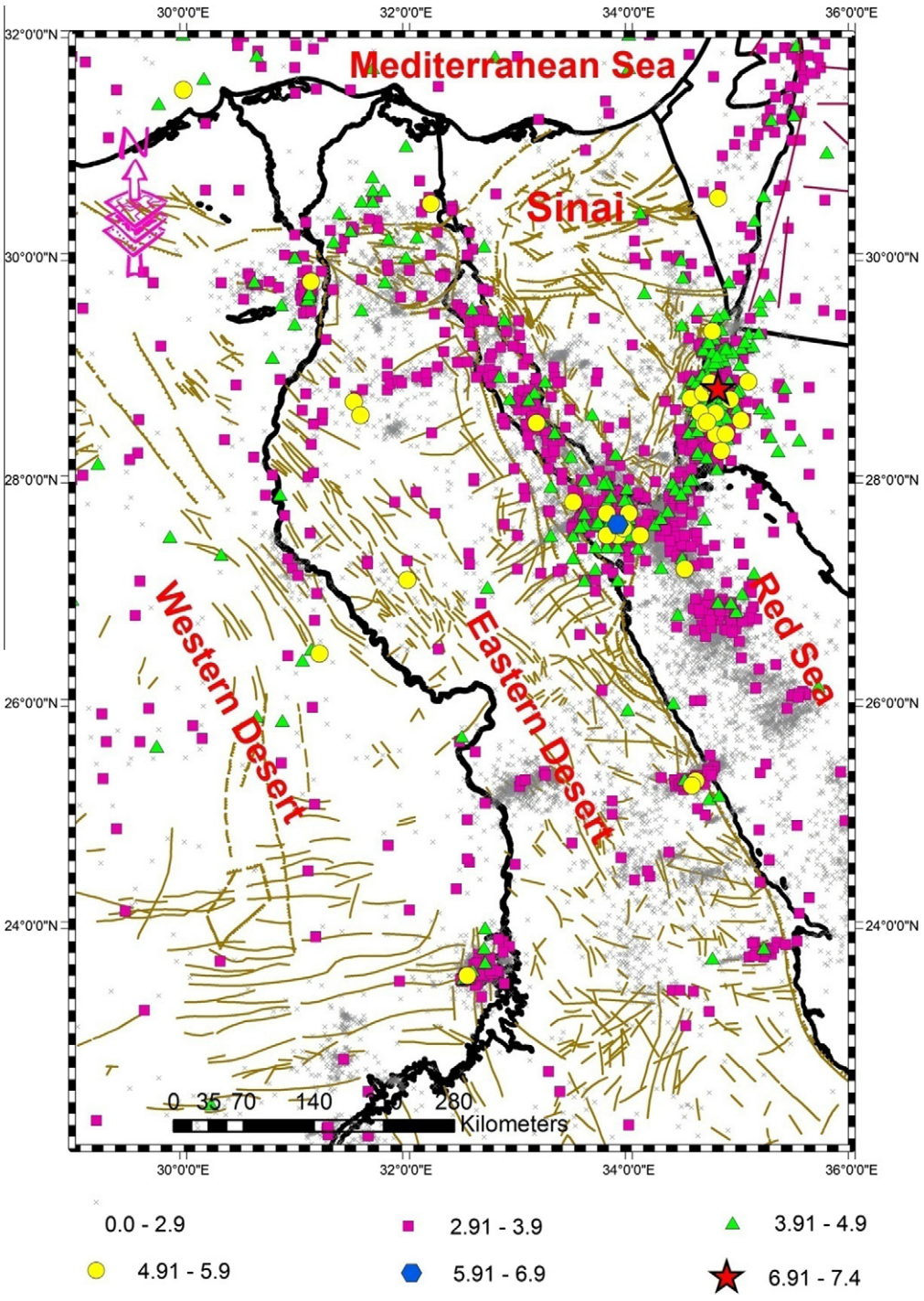

Fig. 8 Seismicity and tectonic setting of the Eastern Desert, (ADB) Abou Dabbab area, (BRS) Barnis Area, (BNS) Beni Seuif area, (CSD) Cairo-Suez district.

fault, which is of prime importance, because it extends towards the High Dam as shown in (Fig. 10).

Seismotectonic model

Seismic zonation studies are very important not only for theoretical studies, but also for practical applications. Both seismic hazard assessment and earthquake prediction depends much on the seismic zonation.

Abou Elenean, 2010 proposed a seismotectonic model for Egypt and its surroundings (Fig. 11). During this study, a new seismotectonic model was proposed, the model is modified After (Papaiouannou and Papazachos (2000), Abdel Rahaman et al. (2008) and Deif et al., 2011), (Fig. 12). Deif et al., 2011, established a detailed seismotectonic model for the area

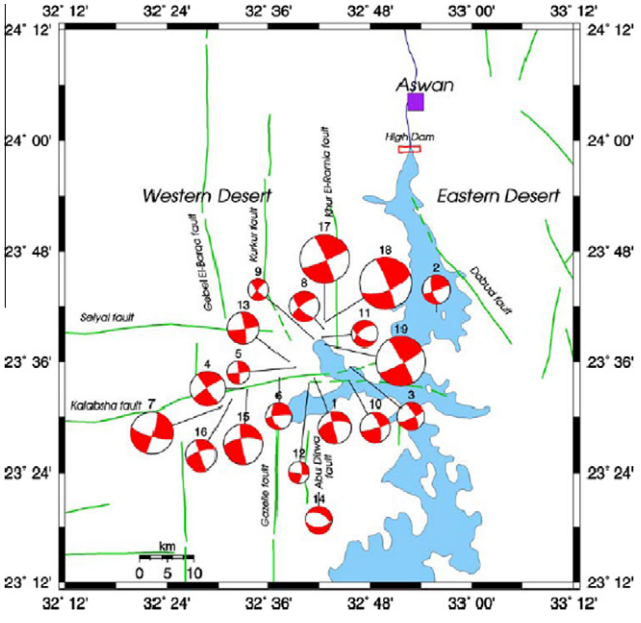

Fig. 9 Focal mechanisms of Aswan area (after Abou Elenean, 2003).

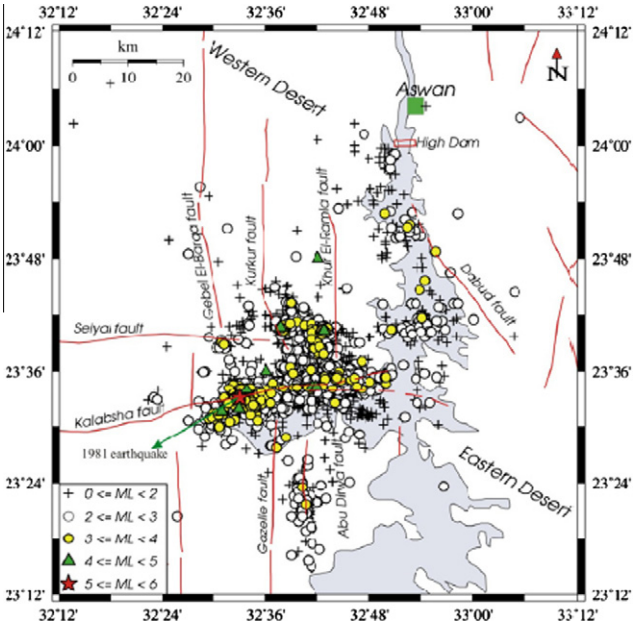

Fig. 10 Seismicty of Aswan area (after Deif et al., 2011).

around Nasser Lake. His classification was based on the available geological, seismological, and geodetic data for the faults around Nasser Lake (Fig. 13).

In the current study the two previously mentioned seismotectonic models are used, in seismic hazard assessment with weights as, the model of Abou Elenean, 2010 is (0.4), while the model that proposed in this study is (0.6) (Fig. 14), this is because both of them were carried out based on actual tectonic setting, focal mechanisms, and seismicity.

Recurrence parameters

The data of the historical catalog was collected from the publications (e.g. Poirier and Taher (1980), Maamoun et al. (1984), Ambraseys et al. (1994), Badawy (1998) and Badawy et al., 2010). Earthquakes with large matter of debate were removed from the seismicity parameters calculations, if an earthquake is occurred in more than one source, some priorities control the choice of a representative earthquake. The first pri-

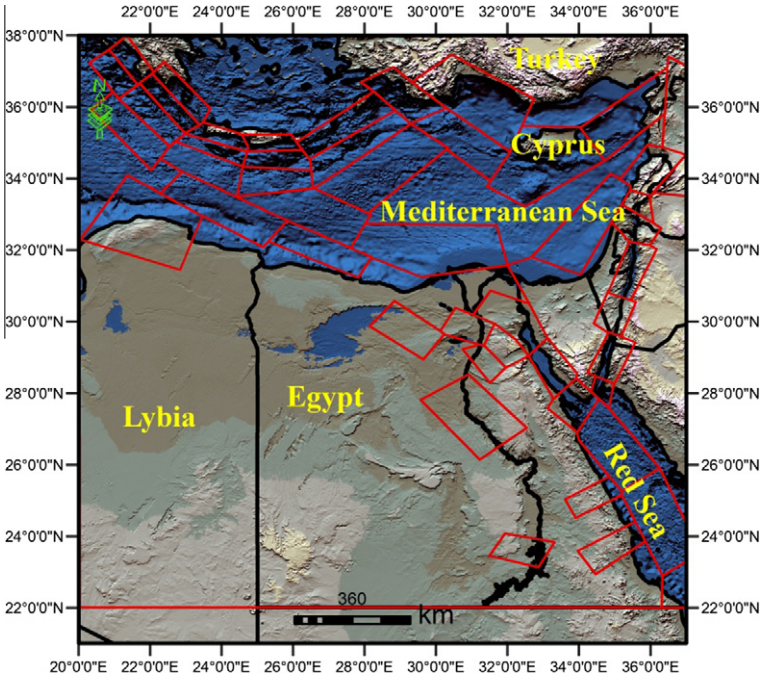

Fig. 11 Seismotectonic model of Egypt and its surrounding (after Abou Elenean, 2010).

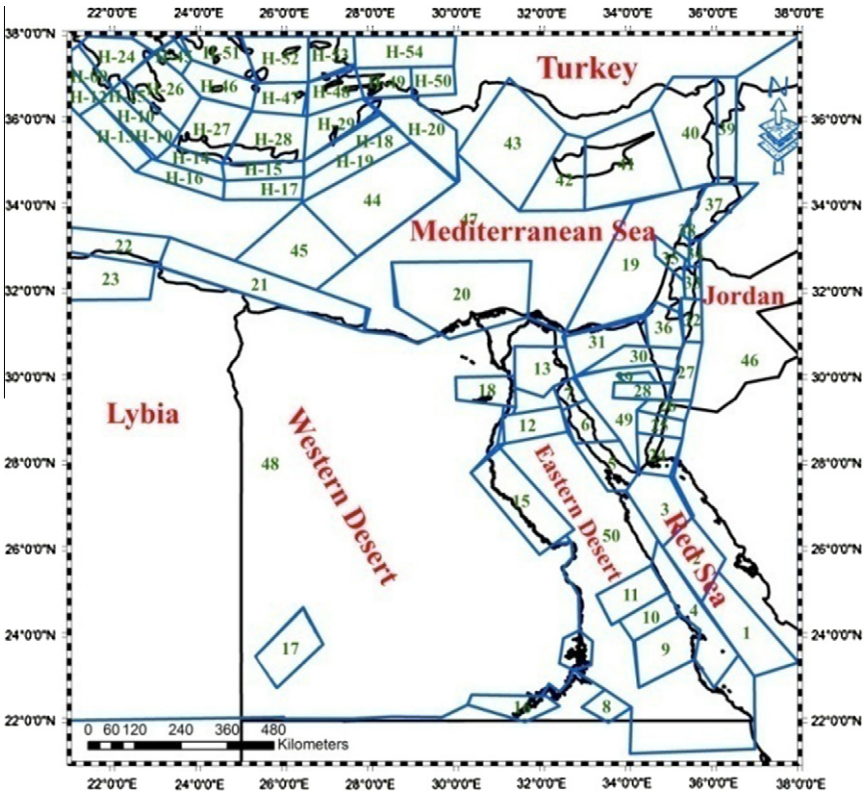

Fig. 12 Delineated seismic sources in and around Egypt, modified after (Papaiouannou and Papazachos (2000), Abdel Rahaman et al. (2008), Deif et al., 2011).

ority was given to Badawy et al., 2010, the second is given to Ambraseys et al. (1994), then to Maamoun et al., 1984; Poirier and Taher, 1980, respectively.

The second part of the catalog is the instrumental part. This part starts in 1900 AD, and continues until now. It is divided into two parts the first part starts in 1900 and ends in 1997, while the second part starts in 1997 (start of the recording of the Egyptian National Seismological Network) and continues until now. It is characterized by the high accuracy in location determination.

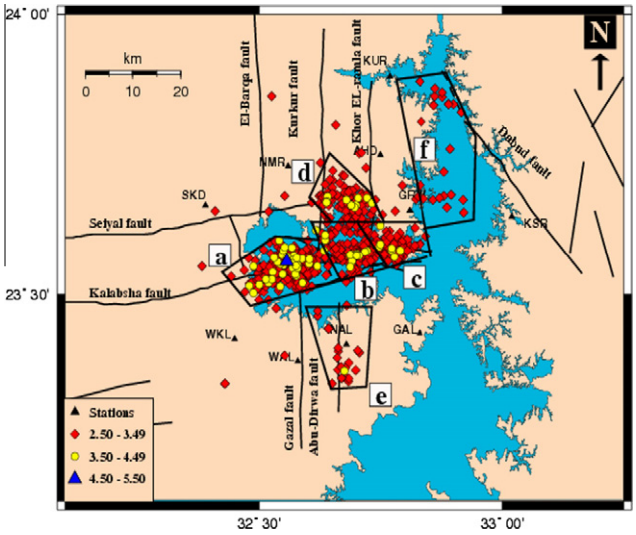

Fig. 13 Seismic sources of Aswan (after Deif et al., 2011).

The instrumental earthquake catalog compiled based on local and international seismological sources. The local sources are Maamoun et al. (1984), Ambraseys et al. (1994) and Abou Elenean (1997) and the bulletin of the Egyptian National Seismological Network during the period from 1997 to 2009. The international sources are the International seismological Center (ISC), Centriod Moment Tensor (CMT), and National Earthquake Information Center (NEIC). If an earthquake was occurred in more than one source, the first priority of earthquake parameter set was given to the Centriod Moment Tensor (CMT) solutions because their determination was based upon the waveform inversion, with a higher accuracy, in addition CMT provides the errors of each parameter. The second priority was given to Ambraseys et al. (1994), since 1997 after the installation of the Egyptian National Seismological Network (ENSN), the first priority was given to the location determinations of the particularly for the earthquakes located inside Egypt.

The catalog was processed by calibrating the magnitude scale into the moment Magnitude using empirical relationships. M_L magnitude of (ENSN) data was converted to the moment magnitude using the equation of Girgis, 2010, Also M_w was estimated from M_s. For 513 events was used and the correlation coefficient of this formula was 0.75 as in Eq. (1) and Fig. 15A.

$$M_w = 0.9137 M_s + 0.05486 \quad (1)$$

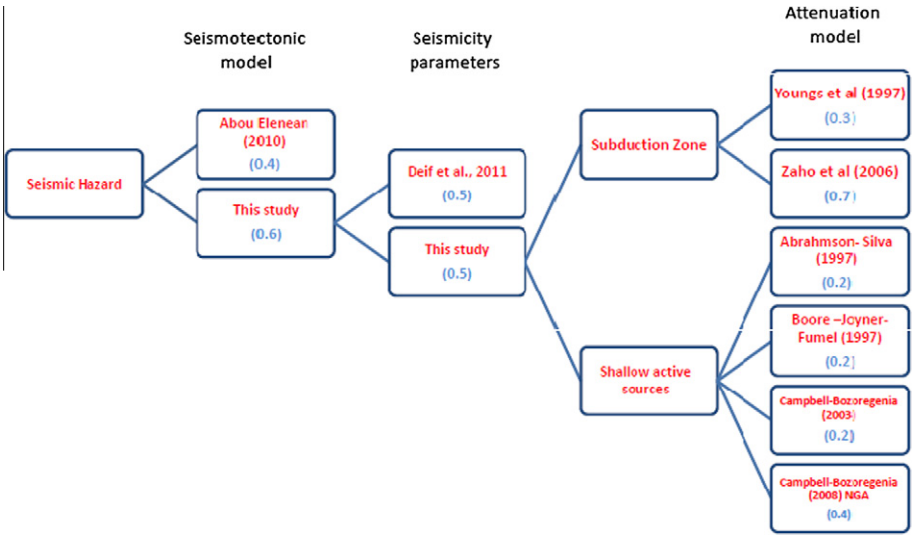

Fig. 14 Components of the logic tree used for hazard calculations, numbers are the assigned weight for each component.

While the second conversion was converting the m_b to M_w, a number of 1273 events were used to deduce this conversion, the correlation coefficient of this formula was 0.76, as in Eq. (2) and Fig. 15B.

$$M_w = 1.1587m_b - 0.8993 \quad (2)$$

(M_w) is considered, because it is the most reliable magnitude scale. Moreover, the ground motion scaling relationships (attenuation) used in the current study are expressed in terms of this magnitude scale.

The second step of processing is removing the repetitions. The third step is catalog declustering to remove dependent events. We applied the Gardner and Knopoff (1974) technique using original parameters given in Gardner and Knopoff (1974). Results of the declustering process show that the contribution of the clusters is 11.37% of the total moment release within the catalog.

To model the seismicity in each zone, we need knowledge on the magnitude of completeness, Mc, below which only a fraction of all events in a magnitude bin are detected by the network (Kijko and Graham, 1999; Rydelek and Sacks, 2003; Wiemer and Wyss, 2000, 2003). Completeness estimates for historical data sets are largely a matter of expert judgment based on an evaluation of various plots of the seismicity. The procedure of Stepp (1972), which is based upon the change of the slope of the cumulative seismicity with time, is used to identify the completeness levels of the catalog.

The results of the completeness analysis for earthquake catalog in Northern Egypt, Gulf of Aqaba–Dead Sea Transform and Cypriot arc show that, the earthquake catalog of Egypt is complete for the earthquakes of magnitude $M_w > 3$ since 1982, and since 1963 for the earthquakes of magnitude $M_w > 3.5$ and for the earthquakes of magnitude $M_w > 5$ complete since 1900 A.D. The catalog of the Cypriot and Hellinic Arcs is complete for the magnitudes $M_w > 3.0$, 4.0 and 5.0 since 1989, 1967 and 1900, respectively. The catalog of the Gulf of Aqaba–Dead Sea transform is complete for the magnitudes $M_w > 3.0$, 3.5, and 5.0 since 1983, 1963, and 1900, respectively.

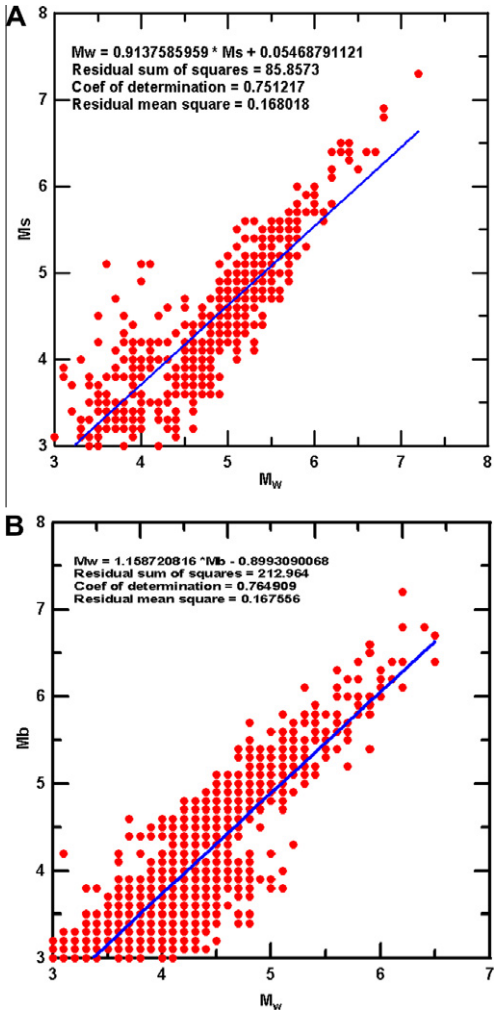

Fig. 15 (A) Conversion of surface-wave magnitude (M_s) into moment magnitude (M_w), based on Harvard catalog. (B) Conversion of body-wave magnitude (m_b) into moment magnitude (M_w), based on Harvard catalog.

Table 1 The seismicity parameters for each seismic zones within the proposed seismotectonic model.

a	SD (b)	*b*	SD (lamda)	Lamda	SD (beta)	Beta	M min	M max	Zone No.	Zone name
4.2	0.04	1.09	0.28	2.2	0.09	2.51	3.5	6.44	(01)	Northern Red Sea Transition Zone (NTR)
3.0	0.06	0.98	0.12	0.39	0.13	2.27	3.5	5.3[a]	(02)	Northern Red Sea Zone (NRS)
3.5	0.23	1.01	0.23	1.01	0.15	2.32	3.5	7.0	(03)	Sinai Triple Junction Zone (STJ)
2.9	0.07	1.0	0.09	0.23	0.16	2.3	3.5	4.9[a]	(04)	Western Red Sea Zone (WRD)
3.0	0.04	0.87	0.26	2.37	0.1	2.0	3.0	6.6	(05)	Southern Gulf of Suez Zone (SGS)
2.5	0.05	0.87	0.08	0.3	0.12	2.0	3.0	6.5[a]	(06)	Middle Gulf of Suez Zone (MGS)
2.4	0.06	0.99	0.15	0.75	0.13	2.28	3.0	4.8[a]	(07)	Northern Gulf of Suez Zone (NGS)
2.1	0.07	0.99	0.138	0.441	0.16	2.28	2.5	4.1	(08)	Allaqi Seismic Zone (ALQ)
2.5	0.07	1.0	0.12	0.34	0.16	2.31	3.0	3.9	(09)	Barnis Seismic Zone (BRS)
2.4	0.07	1.0	0.21	0.98	0.16	2.31	2.5	4.2	(10)	South Abu Dabbab Seismic Zone (SADB)
2.6	0.06	0.97	0.14	0.5	0.13	2.23	3.0	6.1[a]	(11)	Abo Dabbab Seismic Zone (ADB)
3.0	0.07	0.98	0.24	1.05	0.16	2.27	3.0	4.9[a]	(12)	Beni-Seuf Seismic Zone (BNS)
2.2	0.05	0.77	0.1	0.44	0.13	1.78	3.0	5.7[a]	(13)	Cairo-Suez District Zone (CSD)
2.8	0.06	0.97	0.363	2.26	0.14	2.23	2.5	7.08	(14)a	Gabal Marawa Zone (GBM)
2.2	0.07	1.02	0.063	0.447	0.16	2.34	2.5	7.08	(14)b	East-1 Gabal Marawa Zone (EGBM-1)
2.7	0.07	1.03	0.249	1.27	0.16	2.37	2.5	7.08	(14)c	East-2 Gabal Marawa Zone (EGBM-2)
2.7	0.07	1.01	0.269	1.397	0.15	2.33	2.5	6.13	(14)d	Khor El-Ramla Zone (KRL)
1.5	0.06	0.99	0.181	0.099	0.16	2.27	2.5	5.86	(14)e	Abo-Dirwa Zone (ADZ)
2.4	0.05	1.09	0.059	0.507	0.12	2.51	2.5	3.5	(14)f	Old Stream Zone (ODZ)
2.4	0.07	0.95	0.11	0.33	0.16	2.2	3.0	5.6[a]	(15)	Assuit Zone (ASSZ)
1.4	0.07	0.97	0.01	0.01	0.16	2.23	3.0	5.9[a]	(16)	AL-Gilf Al-Kabeer Zone (GLF)
3.0	0.1	0.97	0.1	0.43	0.16	2.24	3.5	6.2	(17)	Dahshour Zone (DSZ)
2.5	0.07	1.02	0.19	0.83	0.16	2.31	2.5	4.2	(18)	Abu Simbl Zone (ASZ)
2.9	0.05	0.93	0.1	0.48	0.12	2.15	3.5	6.7	(19)	Mediterranean Coastal Dislocation Zone (MCDZ)
2.6	0.05	0.91	0.06	0.29	0.1	2.1	3.0	7.2[a]	(20)	North Delta Zone (NDZ)
2.3	0.06	0.88	0.05	0.16	0.13	2.03	3.5	6.3[a]	(21)	Ras EL-Hekma Zone (RHZ)
2.2	0.05	0.93	0.04	0.08	0.13	2.14	3.5	6.6[a]	(22)	Extension of Ras El-Hekma Zone (ERHZ)
1.8	0.0	0.82	0.0	0.15	0.0	1.88	3.0	6.0	(23)	Gabal Al-Akhdar Zone (GAZ)
2.9	0.07	0.91	0.14	0.49	0.16	2.1	3.5	6.6[a]	(24)	Arnona Dakar Zone (ADSZ)
2.7	0.07	0.89	0.17	0.75	0.15	2.05	3.0	7.7[a]	(25)	Aragonese Zone (ASZ)
2.4	0.07	0.9	0.13	0.45	0.07	2.07	3.0	5.6[a]	(26)	Aqaba Zone (AQSZ)
3.1	0.05	0.99	0.2	1.42	0.1	2.28	3.0	7.5[b]	(27)	Wadi-Araba Zone (WAZ)
2.7	0.07	0.94	0.08	0.15	0.16	2.16	3.0	5.2[a]	(28)	Temed Zone (TSZ)
2.2	0.07	1.0	0.07	0.15	0.16	2.31	3.0	4.2[a]	(29)	East Central Sinai (ECSZ)
2.4	0.06	0.98	0.05	0.11	0.13	2.27	3.0	4.9[a]	(30)	Baraq-Paran Seismic Zone (BPSZ)
1.6	0.07	0.99	0.04	0.04	0.16	2.28	3.0	4.4[a]	(31)	Northern Sinai Zone (NSZ)
2.6	0.05	0.9	0.14	0.74	0.1	2.08	3.0	7.5	(32)	Dead-Sea Zone (DSSZ)
2.5	0.06	0.96	0.12	0.43	0.13	2.22	3.0	7.2[b]	(33)	Jordan Valley Zone (JVZ)
2.5	0.07	1.01	0.1	0.3	0.16	2.33	3.0	6.8[b]	(34)	Hula Kineret Zone (HKZ)
1.6	0.07	0.99	0.04	0.04	0.16	2.29	3.0	6.5[b]	(35)	Carmel-Fairi Zone (CFZ)
2.3	0.07	0.99	0.09	0.24	0.15	2.29	3.0	6.6	(36)	Central Palestine Zone (CPZ)
2.3	0.06	0.89	0.1	0.43	0.13	2.06	3.0	7.7[b]	(37)	Lebanon Mountains Zone (LMZ)
2.1	0.06	1.0	0.06	0.14	0.13	2.3	3.0	5.1[a]	(38)	West Lebanon Mountains Zone (WLMZ)
2.0	0.06	0.81	0.1	0.37	0.13	1.87	3.0	7.7[b]	(39)	Ghab Zone (GBZ)
3.2	0.04	0.88	0.21	1.49	0.1	2.03	3.5	7.3	(40)	East Cyprus Zone (ECZ)
3.7	0.04	0.96	0.25	2.03	0.1	2.22	3.5	7.2	(41)	South East Cyprus Zone (SECZ)
3.5	0.05	0.99	0.18	1.1	0.1	2.28	3.5	7.3[a]	(42)	South West Cyprus (SWCZ)
4.2	0.04	1.02	0.37	4.29	0.09	2.35	3.5	6.5	(43)	West Cyprus Zone (WCZ)
4.1	0.05	1.03	0.14	1.04	0.12	2.36	4.0	6.9	(44)	South Crete-1(SCZ-1)
3.2	0.05	0.99	0.13	0.52	0.1	2.28	3.5	6.1[a]	(45)	South Crete-1(SCZ-2)
2.6	0.04	0.76	0.06	0.4	0.1	1.74	4.0	7.2	(46)	Easter Back Ground Seismicity Zone
3.4	0.06	1.02	0.06	0.2	0.13	2.34	4.0	6.2[a]	(47)	Mediterranean Background Seismicity Zone
3.0	0.07	0.99	0.09	0.4	0.16	2.28	3.5	5.6	(48)	Western Background Seismicity Zone
2.6	0.07	0.96	0.06	0.19	0.16	2.21	3.5	5.8[a]	(49)	Sinai Background Seismicity Zone
3.5	0.05	1.01	0.14	1.02	0.12	2.33	3.5	7.0[a]	(50)	Eastern Desert Background Seismicity Zone
3.7	0.15	0.94	0.15	0.98	0.15	2.17	4.0	6.3[a]	(H-09)	Hellenic Arc-09
3.5	0.06	0.89	0.16	1.02	0.15	2.05	4.0	6.28	(H-10)	Hellenic Arc-10
3.8	0.06	1.04	0.1	0.49	0.13	2.38	4.0	5.6	(H-12)	Hellenic Arc-12
4.3	0.05	1.05	0.15	1.16	0.12	2.42	4.0	7.25	(H-13)	Hellenic Arc-13
3.3	0.05	0.87	0.11	0.63	0.12	2.01	4.0	6.6	(H-14)	Hellenic Arc-14
3.9	0.07	0.97	0.16	1.14	0.15	2.24	4.0	5.89	(H-15)	Hellenic Arc-15
4.0	0.05	0.98	0.15	1.12	0.12	2.27	4.0	7.8[a]	(H-16)	Hellenic Arc-16
3.4	0.05	0.82	0.16	1.3	0.11	1.89	4.0	6.26	(H-17)	Hellenic Arc-17

(*continued on next page*)

Table 1 (*continued*)

a	SD (b)	*b*	SD (lamda)	Lamda	SD (beta)	Beta	M min	M max	Zone No.	Zone name
3.6	0.05	0.87	0.16	1.28	0.11	2.0	4.0	7.8	(H-18)	Hellenic Arc-18
4.1	0.05	1.0	0.15	1.14	0.12	2.3	4.0	5.98	(H-19)	Hellenic Arc-19
3.2	0.05	0.83	0.13	0.86	0.12	1.92	4.0	8.1[a]	(H-20)	Hellenic Arc-20
4.3	0.05	1.05	0.16	1.32	0.12	2.43	4.0	7.6[a]	(H-24)	Hellenic Arc-24
3.4	0.05	0.9	0.11	0.59	0.12	2.08	4.0	8.0[a]	(H-25)	Hellenic Arc-25
4.0	0.05	1.01	0.14	1.04	0.12	2.33	4.0	8.2[a]	(H-26)	Hellenic Arc-26
4.0	0.05	1.01	0.13	0.91	0.12	2.33	4.0	7.4	(H-27)	Hellenic Arc-27
3.6	0.05	0.88	0.15	1.21	0.11	2.02	4.0	7.8	(H-28)	Hellenic Arc-28
3.8	0.05	0.93	0.16	1.28	0.11	2.15	4.0	7.9[a]	(H-29)	Hellenic Arc-29
3.0	0.07	0.91	0.07	0.21	0.16	2.09	4.0	6.8[a]	(H-44)	Hellenic Arc-44
3.1	0.07	0.97	0.06	0.17	0.16	2.23	4.0	5.38	(H-45)	Hellenic Arc-45
3.3	0.06	0.95	0.08	0.3	0.13	2.19	4.0	6.57	(H-46)	Hellenic Arc-46
3.9	0.05	0.99	0.13	0.81	0.12	2.29	4.0	7.9[a]	(H-47)	Hellenic Arc-47
3.7	0.05	0.92	0.14	1.07	0.11	2.11	4.0	8.3[a]	(H-48)	Hellenic Arc-48
3.2	0.14	0.83	0.07	0.83	0.15	1.92	4.0	5.74	(H-49)	Hellenic Arc-49
3.3	0.07	0.94	0.09	0.33	0.16	2.17	4.0	6.0[a]	(H-50)	Hellenic Arc-50
3.1	0.07	0.99	0.06	0.14	0.16	2.27	4.0	6.5[a]	(H-51)	Hellenic Arc-51
3.1	0.07	0.98	0.06	0.16	0.16	2.25	4.0	6.3[a]	(H-52)	Hellenic Arc-52
3.2	0.07	0.9	0.1	0.4	0.16	2.07	4.0	6.5[a]	(H-53)	Hellenic Arc-53
3.5	0.05	0.91	0.13	0.81	0.12	2.1	4.0	5.86	(H-54)	Hellenic Arc-54

The parameters of zones 8, 10, 14-a to 14-f, and 18 after (Deif et al., 2011).When not specified, maximum magnitude based upon Kijko (2004).
a Maximum magnitude calculated from the maximum observed magnitude + 0.5.
b Maximum magnitude (after Deif et al., 2009) based upon available paleoseismic studies.

Estimation of the activity parameters β and k

The seismicity of a seismogenic zone is quantified in terms of the recurrence relationship

$$\log N(M_w) = a - b(M_w)$$

where, N is the number of earthquakes of magnitude M or greater per unit time. The a value is the activity and defines the intercept of the above recurrence relationship (Gutenberg and Richter 1944) at M equals zero.

The number of occurrences per year of a hazardous event (e.g. the annual frequency that the ground-motion parameter, X, at a site exceeds a specified value x) is defined as the annual frequency and usually denoted as $\lambda(X \geqslant x)$. The parameter b is the slope, which defines the relative proportion of small and large earthquakes.

In the current study, all seismic sources were assumed to generate earthquakes according to a doubly bounded exponential distribution (Cornell and Vanmarcke 1969). This is because the Gutenberg and Richter (1944) relationship imposes the unrealistic assumption that the maximum potential earthquake for any region under consideration is unbounded and unrelated to the seismotectonic setting. The following truncated exponential recurrence relationship is therefore commonly used in practice:

$$N(\geqslant M) = \alpha \frac{\exp[-\beta(M - M_{\min})] - \exp[(M_{\max} - M_{\min})]}{1 - \exp[-\beta(M_{\max} - M_{\min})]},$$

where $\alpha = N(M_{\min})$, $M_{\min}$ is an arbitrary reference magnitude, $M_{\max}$ is an upper-bound magnitude where

$N(m) = 0 \, for \, M > M_{\max}$, and $\beta = b \cdot \ln 10$.

In this form, earthquake frequency approaches zero for some chosen maximum earthquake of a region. The compiled catalog has varying levels of completeness and these must be accounted for when deriving activity parameters for the seismic sources. The parameters of the doubly bounded exponential distribution were obtained in this study using the maximum likelihood estimation procedure of Weichert (1980).

Maximum magnitude determination was estimated based on the previous seismological and paleoseismological studies, or by adding 0.5 for the maximum observed magnitude within the seismic zone. Concerning seismic sources with enough data the maximum magnitude was calculated using statistical procedure of Kijko (2004). The seismicity parameters are shown in (Table 1). Changing in zones boundaries between the two used seismotectonic models lead to change in the magnitude of the maximum observed earthquake. For example, the zone of Cairo-Suez-District that is defined by the current study has a maximum observed earthquake with magnitude moment 5.2, 1 Feb, 1982 event. The same zone based on Abou Elenean (2010) seismotectonic model has a maximum observed magnitude of (6.6 M_F), which of a historical event of the 1754 A.D (northern part of the Gulf of Seuz).

Attenuation models

Alternative ground-motion scaling relationships are here applied to various tectonic provinces considered in the current study to account for the epistemic uncertainty associated with not knowing the true attenuation characteristics from each

seismogenic zones to the sites of Egypt. Six different ground-motion scaling relationships were considered following the guidelines proposed by Cotton et al. (2006). These models were extensively used in seismic hazard assessment in different places in the world. In the current study, the models of Youngs et al. (1997) and Zhao et al. (2006). Were used to model the ground-motions from subduction seismic sources such as the sources of the Cyprean and Hellenic arcs. The models of Abrahmson and Silva (1997), Boore et al. (1997), Campbell and Bozorgnia (2003) and Campbell and Bozorgnia (2008), were used with ground-motions of earthquakes occurring within the active shallow crust seismogenic zones. The assigned weight for each ground-motion prediction equation is shown in the logic tree (Fig. 14).

Hazard calculations

Conventional seismic hazard mapping based on the probabilistic model is carried out in the present study. The probabilistic seismic hazard analyses have been generally conducted in Egypt, and especially for Cairo, and Alexandria. The objective was to evaluate the probability of exceedance for different levels of ground motion. The probabilistic approach is used to assess the seismic hazard of the studied area using the area source model. Uncertainties, due to errors associated with the delineation of the source boundary and attenuation model, are mindfully treated using the logic tree formulation (Fig. 14). Numerical calculations are done utilizing the Crisis 2007, (Ordaz et al., 2007), computer program. The seismic hazard is calculated for different return periods 475, and 2475 years. The resulted seismic Hazard maps are presented in different spectral periods 0.03 (PGA), 0.1, 0.2, 0.3, and 1 s.

Seismic hazard values are calculated over $0.5° \times 0.5°$ grid extending allover Egypt and its close surroundings, for a total number of 620 computation points as shown in (Fig. 4).

Results

Results of the probabilistic seismic assessment of Egypt using the logic-tree framework are treated to obtain at each point the mean value of the acceleration. The PGA and 5% damped horizontal spectral acceleration values at 0.1, 0.2, 0.3 and 1 s spectral periods were mapped so that can be used to generate an approximate Uniform Hazard Spectrum (UHS) for each point on the hazard maps for the range of periods important for common engineering structures.

The hazard maps displaying the regional distribution of the mean ground-motion in cm/s^2 for a rock condition, with 10%, and 2% probability of exceedance in 50 years, which correspond to return periods 475, and 2475 years respectively Figs. 16–25.

The iso-acceleration maps delineated the Gulf of Aqaba region of relatively highest seismic hazard in the country, which is characterized by moderate seismic activity. The second active area is the entrance of the Gulf of Suez. In the southern part of Egypt high seismic activity is noticed around Aswan area. Also there are some areas with noticed relatively higher seismic activity than their surroundings as Dahshour area, the area of Cairo Suez District, Beni-Seuf area, and Abou-Dabbab area. Generally the acceleration values within the Eastern Desert are higher than the acceleration values of the Western Desert, which is characterized by very low seismic activity, as shown in (Figs. 16–25). The PGA across Egypt ranges between 25 cm/s^2 in middle part of the Western Desert and 220 cm/s^2 in the most northeastern part of Egypt near the area of the source of Gulf of Aqaba earthquake with moment magnitude 7.2 for 475 year return period, and between 50 and 400 cm/s^2 for 2475 year return period. The pattern of hazard is closely related to the geometry of the seismic source zones adopted. As the return period increases, the acceleration value at particular place proportionally increases. The response spectra of Cairo show that the PGA values are 40, 80, 100, 130 gal for return periods 72, 475, 975 and 2475 years return periods (Fig. 26a). Concerning Alexandria the PGA values are 30, 50, 60, 80 gal for return periods 72, 475, 975 and 2475 years return periods (Fig. 26b).

The results of the present study are compared with those of the Global Seismic Hazard Assessment Program (GSHAP), which was developed based on more generalized seismotectonic model in lack of specific and detailed seismic zonation. The (GSHAP) map is calculated for a 90% probability of not being exceeded in 50 years on rock (475 years return period). Our results are similar as the generalized (GSHAP) map showing a relatively high hazard values at the Gulf of Aqaba, Gulf of Suez and Aswan area. It compares well with the hazard values in this study, taking into consideration the uncertainty in reading values off the more generalized GSHAP map. Detailed probabilistic seismic hazard assessment is carried out for some important cities in Egypt as Cairo, Alexandria, as they are of socio-economic importance. The calculated seismic hazard curves of each seismic source for Cairo show that, Cairo is mainly affected by Dahshour area, and Cairo Suez District. Also, Alexandria is mainly affected by the North Delta Zone (zone No. 20) and intermediate depth earthquakes which occur in the Hellenic Arc.

Summary and conclusion

The present study is focus on studying the seismic hazard of Egypt. It presents seismic hazard maps for Egypt for 475 and 2475 years return periods for different spectral acceleration values, in case of rock sites conditions. The Uniform Hazard Spectra (UHS) for Cairo and Alexandria were also estimated. A grid, of 621 points represents $(0.5° \times 0.5°)$ degree covering Egypt, is used for calculating the seismic hazard. The produced seismic hazard maps provide the civil engineers information about the spectral value for each period and then the capability construct a UHS for his proposed site. The produced UHS curves for Cairo and Alexandria cities describe the seismic hazard in terms of building height that reflect the real levels of hazard at all frequencies. Engineers are interested in the spectral periods range between 0.1 and 1 s., which are shown in the current study for Cairo and Alexandria cities. The uncertainty analysis is estimated during the seismic hazard calculations. Statistical variability in the ground-motion prediction relationships and in delineation of the source boundaries is among the most significant source of uncertainty. The results of this study are the main input for studying the seismic risk, which yields deterministic or probabilistic estimates of the expected loss of properties and lives.

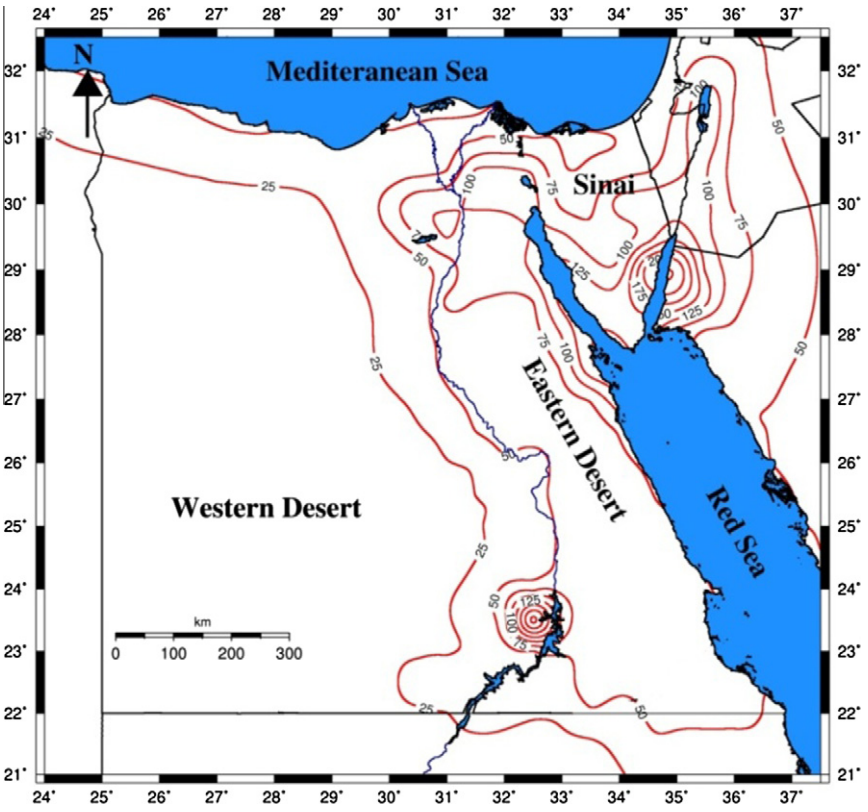

Fig. 16 Mean peak ground acceleration (cm/s^2) on rock sites with 10% probability of exceedance in 50 year (475 year return period) in Egypt.

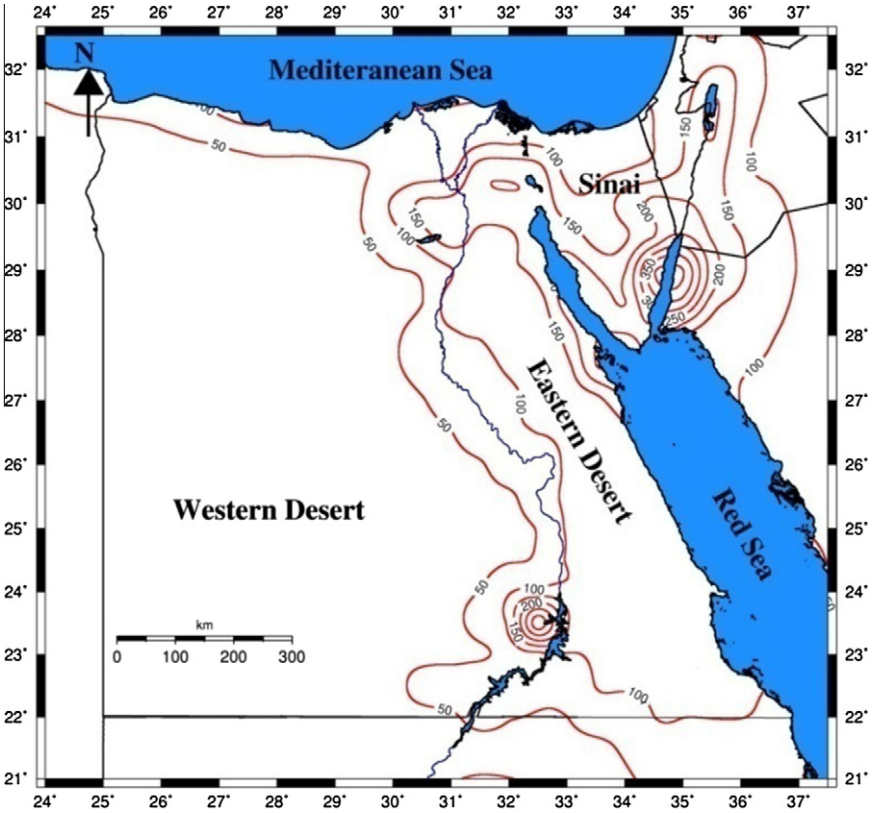

Fig. 17 Mean peak ground acceleration (cm/s^2) on rock sites with 2% probability of exceedance in 50 year (2475 year return period) in Egypt.

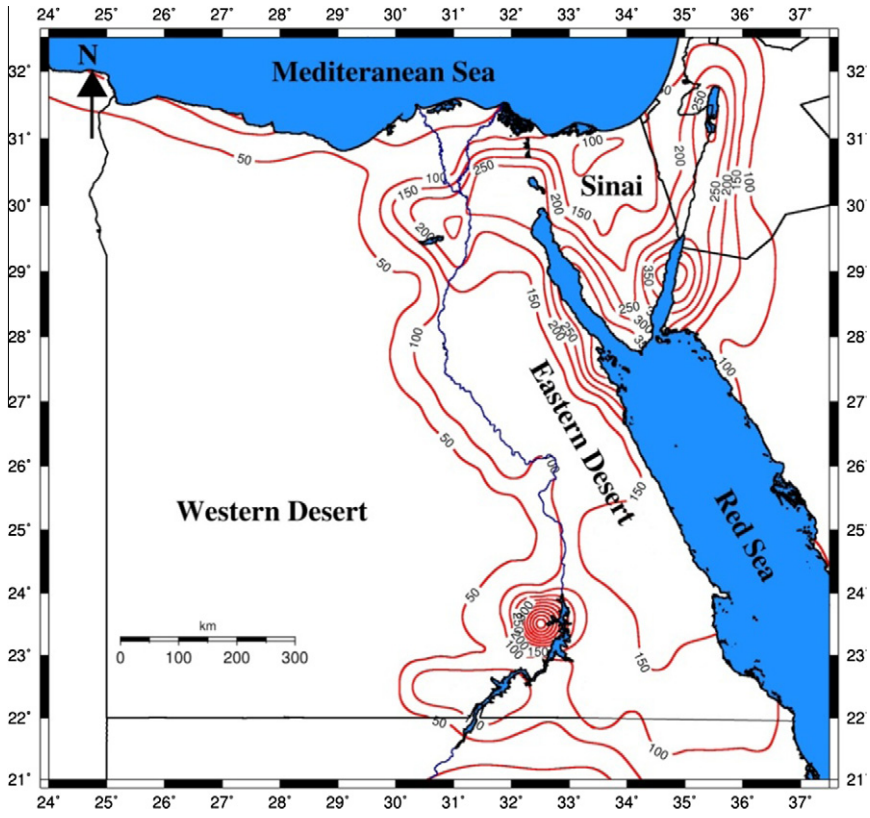

Fig. 18 5% Damped mean spectral acceleration for 0.1 s spectral period (cm/s^2) on rock sites with 10% probability of exceedance in 50 year (475 year return period) in Egypt.

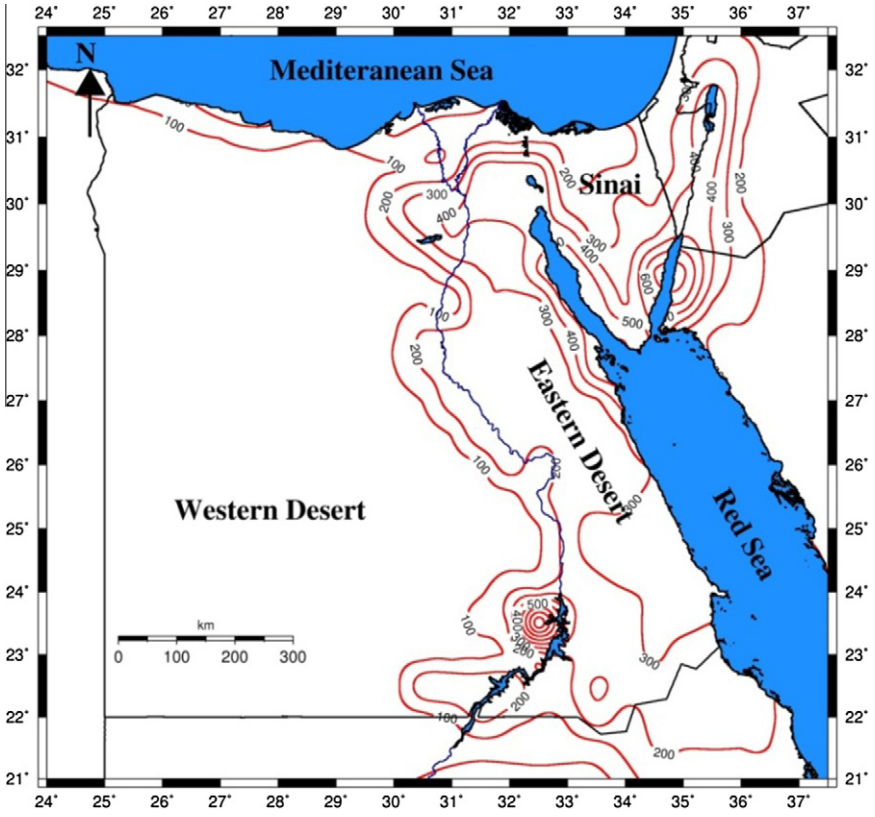

Fig. 19 5% damped mean spectral acceleration for 0.1 s spectral period (cm/s^2) on rock sites with 2% probability of exceedance in 50 year (2475 year return period) in Egypt.

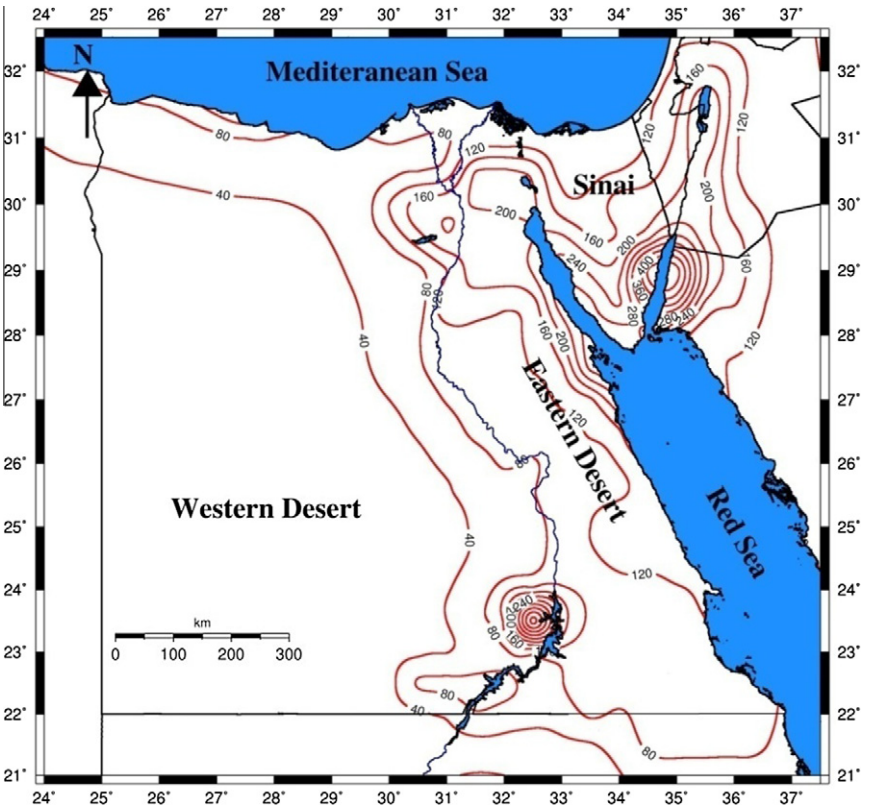

Fig. 20 5% damped mean spectral acceleration for 0.2 s spectral period (cm/s^2) on rock sites with 10% probability of exceedance in 50 year (475 year return period) in Egypt.

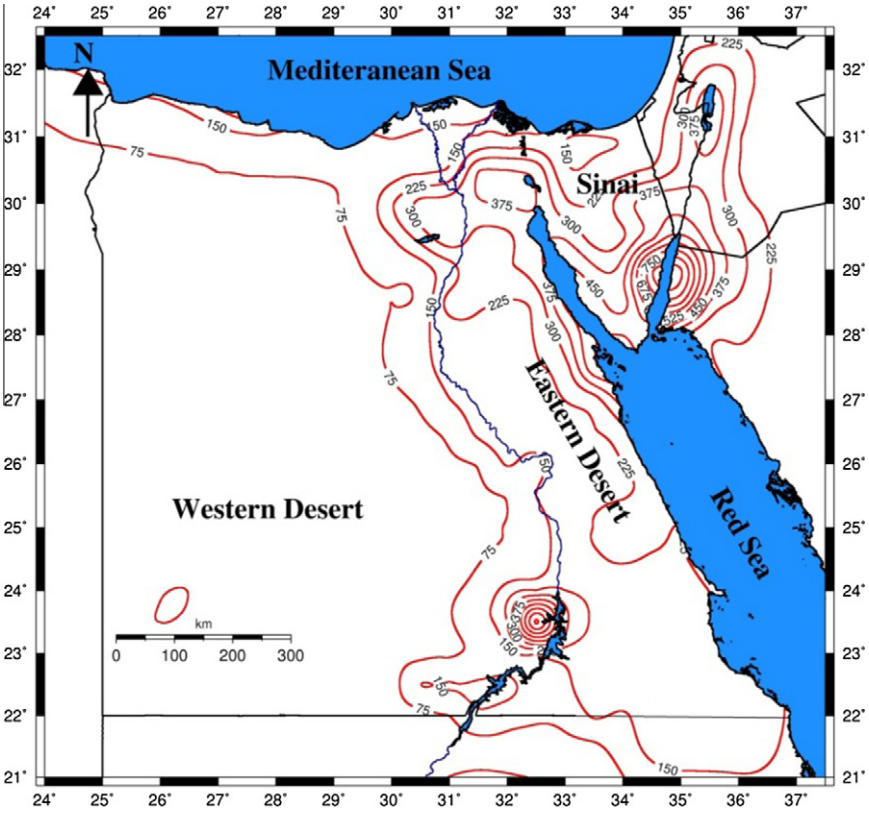

Fig. 21 5% damped mean spectral acceleration for 0.2 s spectral period (cm/s^2) on rock sites with 2% probability of exceedance in 50 year (2475 year return period) in Egypt.

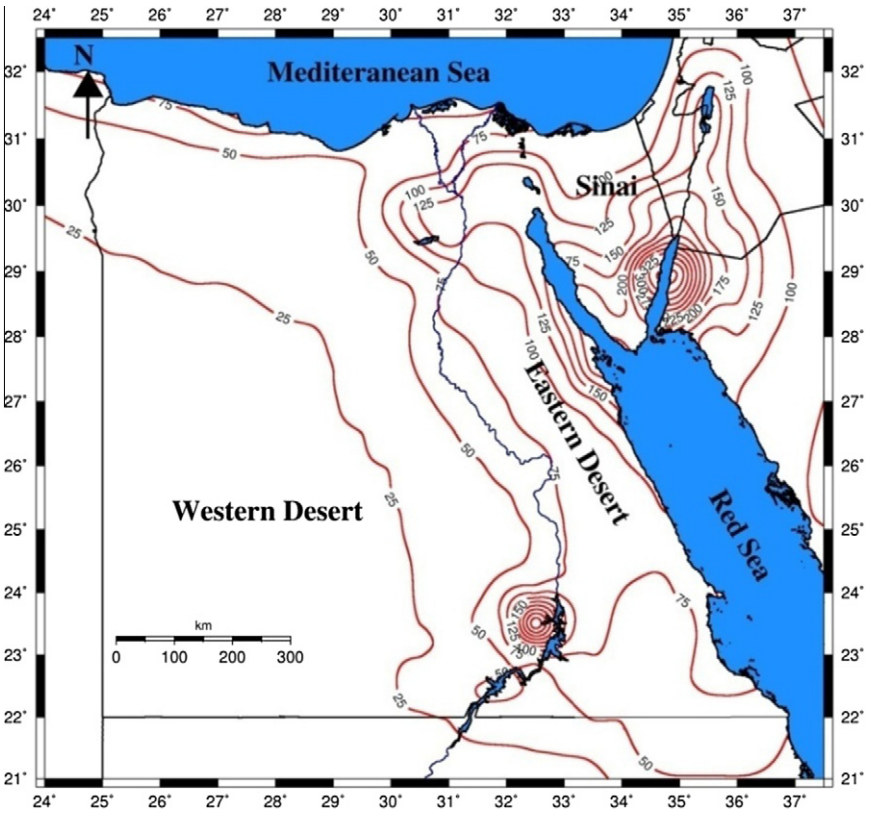

Fig. 22 5% damped mean spectral acceleration for 0.3 s spectral period (cm/s^2) on rock sites with 10% probability of exceedance in 50 year (475 year return period) in Egypt.

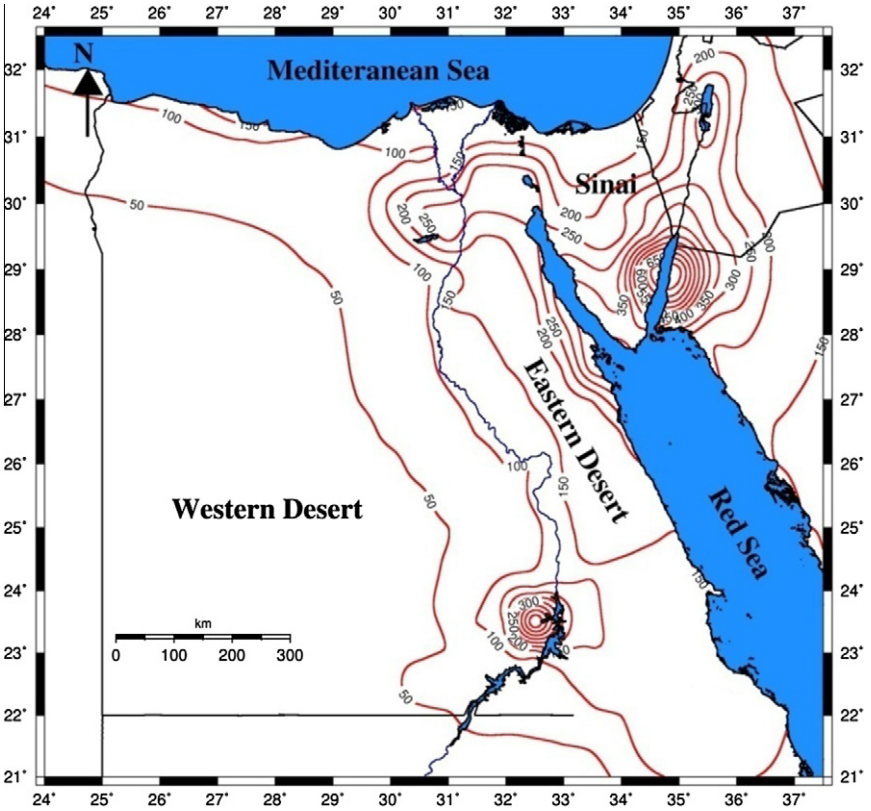

Fig. 23 5% damped mean spectral acceleration for 0.3 s spectral period (cm/s^2) on rock sites with 2% probability of exceedance in 50 year (2475 year return period) in Egypt.

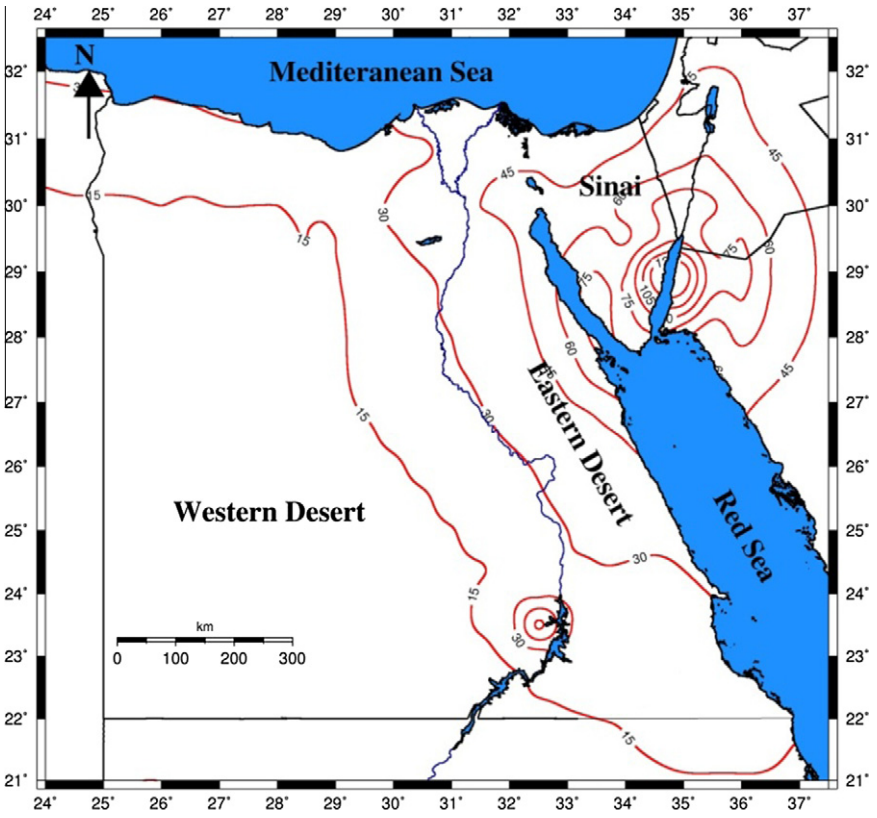

Fig. 24 5% damped mean spectral acceleration for 1 s spectral period (cm/s^2) on rock sites with 10% probability of exceedance in 50 year (475 year return period) in Egypt.

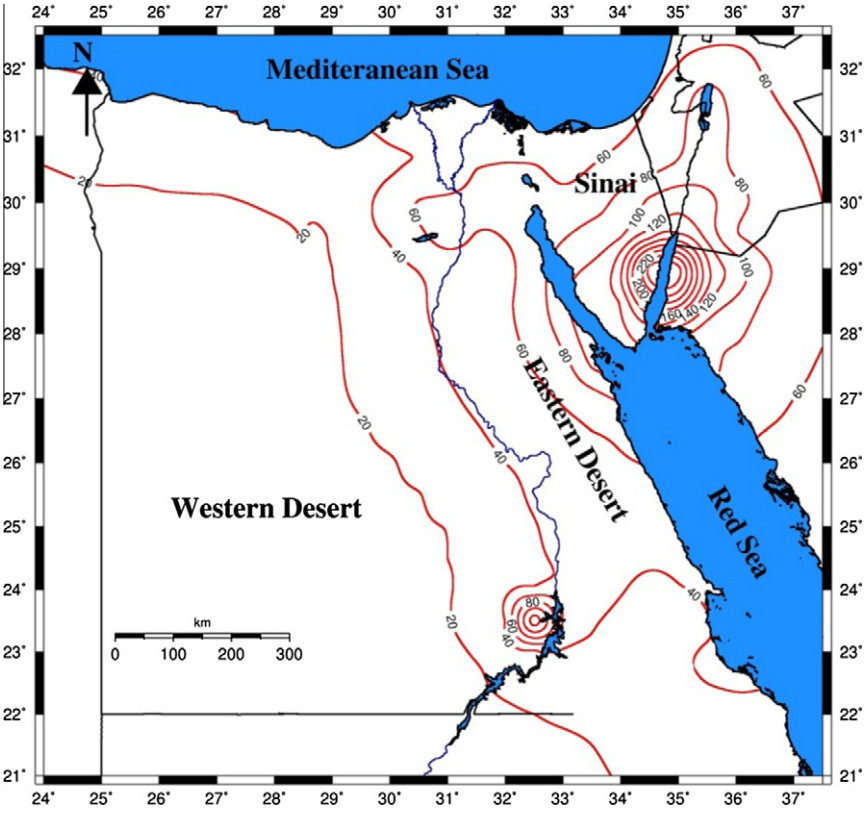

Fig. 25 5% damped mean spectral acceleration for 1 s spectral period (cm/s^2) on rock sites with 2% probability of exceedance in 50 year (2475 year return period) in Egypt.

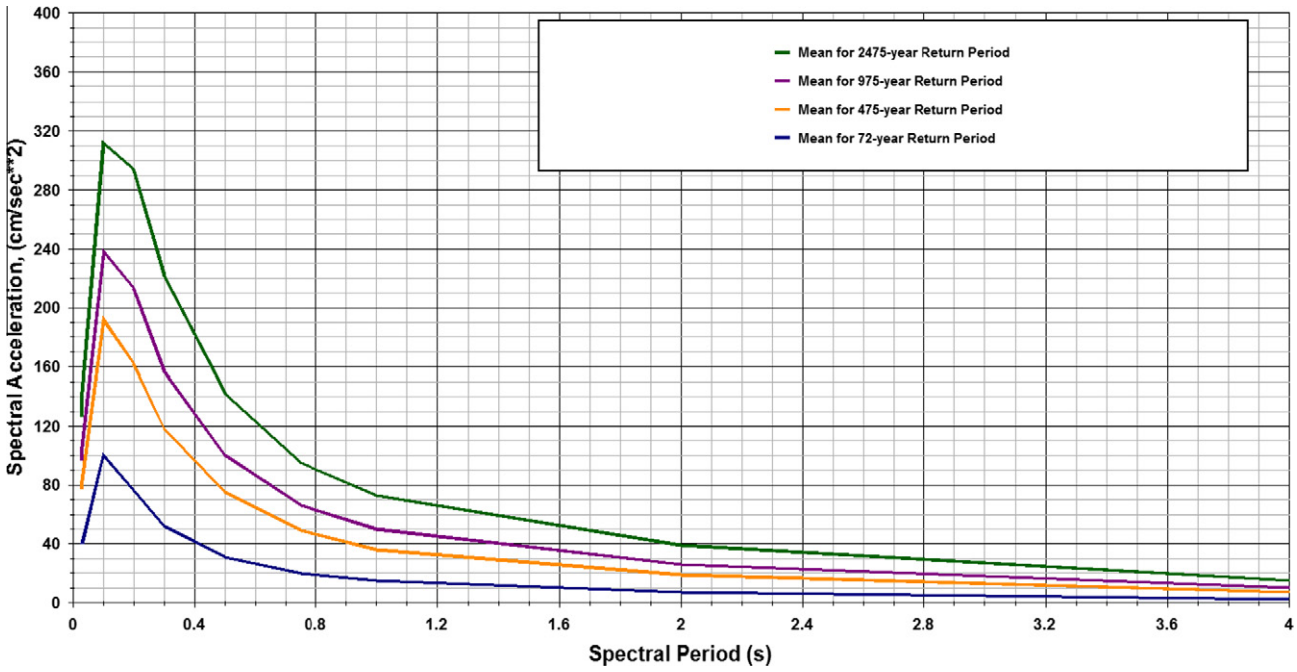

Fig. 26a Unified hazard spectra for the rock sites of 72, 475, 975 and 2475 years return period in Cairo city.

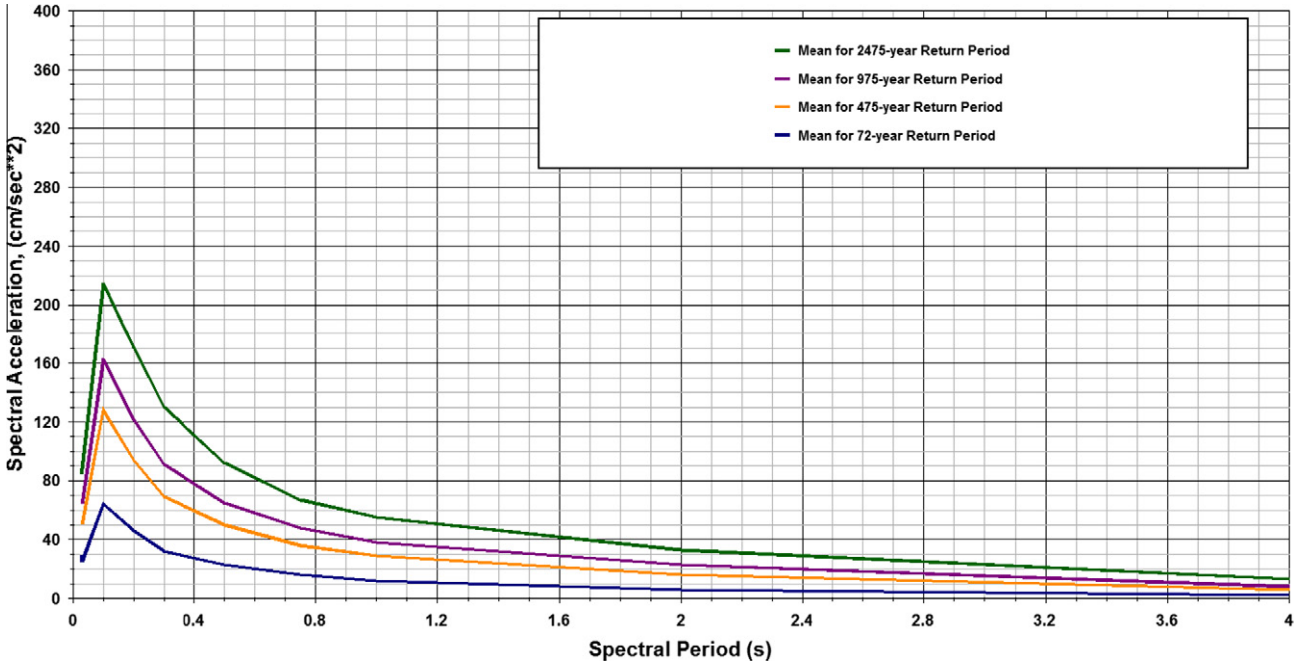

Fig. 26b Unified hazard spectra for the rock sites of 72, 475, 975 and 2475 years return period in Alexandria city.

References

Abd El-Tawb, S., Helal, S., Deweidar, H., El-Sayed, A., A., 1993. Surface tectonic features of 12 Oct., 1992 earthquake, Egypt, at the epicentral area. Ain Shams Sci. Bull., 124–136 (Special issue 1993).

Abdel Rahaman, M., Tealeb, A., Mohamed, A., Deif, A., Abou Elenean, K., El-Hadidy, M.S., 2008. Seismotectonic zones at Sinai and its surrounding. In: First Arab Conference on Astronomy and Geophysics, Helwan, Egypt, 20–22 October 2008.

Abdel-Fattah, A.K., Hussein, H.M., Ibrahim, E.M., Abu El Atta, A.S., 1997. Fault plane solutions of the 1993 and 1995 Gulf of Aqaba earthquakes and their tectonic implications. Ann. Geofis. 40, 1555–1564.

Abou Elenean, K., 1997. Seismotectonics of Egypt in relation to the Mediterranean and Red Seas tectonics. Ph. D. Thesis. Fac. Sc. Ain Shams Univ., pp. 200.

Abou Elenean, K., 2010. Seismotectonics Studies of El-Dabaa and its surroundings, personal communication.

Abou Elenean, K., 1993. Seismotectonics of the Mediterranean region north of Egypt and Libya, M. Sc. Thesis. Fac. of Sci., Mansoura Univ., Egypt, pp. 198.

Abou Elenean, K., 2004. Seismological aspects of the Eastern Mediterranean region, RA.

Abou Elenean, K., Hussien, H.M., 2008. The October 11, 1999 and November 08, 2006 Beni Suef earthquakes. Pure Appl. Geophys. 165, 1391–1410.

Abou Karaki, N., Dorbath, L., Haessler, H., 1993. La crise sismique du golfe d'Aqaba de 1983: implication tectonique.. C. R. Acad. Sci., Paris 317, 1411–1416.

Abrahmson, N.A., Silva, W.J., 1997. Empirical response spectra attenuation relations for shallow crustal earthquakes, Seismo. Res. Lett. 68, 94–127.

Aksu, A.E., Hall, J., Yaltirak, C., 2005. Editorial: miocene to recent tectonic evolution of Eastern Mediterranean: new pieces of the old Mediterranean puzzle. Mar. Geol. 221, 1–13.

Alamri, A., Scholt, F., Bufe, C., 1991. Seismicity and aeromagnetic features of the Gulf of Aqaba (Elat) region. J. Geophys. Res. 96, 20179–20185.

Ambraseys, N.N., Melville, C.P., Adams, R.D., 1994. The seismicity of Egypt, Arabia and Red Sea. Cambridge Univ. Press.

Badawy, A., 1998. Earthquake hazard analysis in northern Egypt. Acta Geod. Geophys. Hung. 33, 341–357.

Badawy, A., Horvath, F., 1999. Recent stress field of the Sinai subplate region. Tectonophysics 304, 385–403.

Badawy, A., Al-Gabry, M., Girgis, M., 2010. Historical seismicity of Egypt. In: A Study for Previous Catalogues Producing Revised Weighted Catalogue the Second Arab Conference for Astronomy and Geophysics, Egypt.

Ben-Avraham, Z., 1985. Structural framework of the Gulf of Elat (Aqaba). J. Geophys. Res. 90, 703–726.

Ben-Avraham, Z., Shoham, Y., Ginzburg, A., 1976. Magnetic anomalies in the Eastern Mediterranean and the tectonic setting of the Eratosthenes Seamount. Geophys. J. Res. Astron. Soc. 45, 105–123.

Ben-Avraham, Z., Almagor, G., Garfunkel, Z., 1979. Sediments and structure of the Gulf of Elat (Aqaba) northern Red Sea. Sediment. Geol. 23, 239–267.

Ben-Avraham, Z., Nur, A., 1986. Collisional processes in the Eastern Mediterranean. Geol. Rundsch., 209–217.

Ben-Avraham, Z., Kempler, D., Ginzburg, A., 1988. Plate convergence in the Cyprean arc. Tectonophysics 146, 231–240.

Boore, D.M., Joyner, W.B., Fumal, T.E., 1997. Equations for estimating horizontal response spectra and peak acceleration from western north american earthquakes: a summary of recent work. Seismol. Res. Lett. 68, 128–153.

Campbell, K.W., Bozorgnia, Y., 2003. Updated near-source ground motion (attenuation) relations for the horizontal and vertical components of peak ground acceleration and acceleration response spectra. Bull. Seismol. Soc. Am. 93 (1), 314–331.

Campbell, K.W., Bozorgnia, Y., 2008. NGA ground motion model for the geometric mean horizontal component of PGA, PGV, PGD and 5% damped linear elastic response spectra for periods ranging from 0.01 to 10 s, earthquake spectra. Earthq. Eng. Res. Inst. 24 (1), 139–171.

CMT, Centroid Moment Tensor Catalog. Available from: <http://www.seismology.harvard.edu.>

Cochran, J.R., Martinez, F., 1988. Evidence from the northern Red Sea on the transition from continental to oceanic rifting. Tectonophysics 153, 25–53.

Cochran, J.R., Martinez, F., Steckler, M.S., Hobart, M.A., 1986. Conrad deep, a new northern Red Sea deep, origin and implications for continental rifting. Earth Planet. Sci. Lett. 78, 18–32.

Comninakis, P., Papazachos, B., 1972. Seismicity of the Eastern Mediterranean and some tectonic features of the Mediterranean ridge. Geol. Soc. Am. Bull. 83, 1093–1102.

Comninakis, P., Papazachos, B., 1980. Space and time distribution of the intermediate focal depth earthquakes in the Hellenic arc. Tectonophysics 70, 35–47.

Cornell, C.A., Vanmarcke, E.H., 1969. The major influences on seismic risk. In: Proceedings of the Fourth World Conference of Earthquake Engineering, vol. 1. Santiago, Chile, pp. 69–83.

Cotton, F. et al, 2006. Criteria for selecting and adjusting ground-motion models for specific target applications: applications to Central Europe and rock sites. J. Seismol. 10, 137–156.

Daggett, P., Morgan, P., Boulous, F., Hennin, S., El-Sherif, A., El-Sayed, A., Basta, N., Melek, Y., 1986. Seismicity and active tectonics of the Egyptian Red Sea margin and the northern Red Sea. Tectonophysics 125, 313–324.

Deif, A., Hamed, H., Ibrahim, H.A., Abou Elenean, K., El-Amin, E., 2011. Seismic hazard assessment in Aswan Egypt. J. Geophys. Eng. 8 (2011), 531–548.

Egyptian Geological Survey an Mining Authority, 1996. Geology of Pan-African basement rocks of Jabal Al-Hadid-Wadi Mubark Distrct, Egypt.

El Hadidy, M., 2008. Seismotectonics and seismic hazard studies for Sinai Peninsula, Egypt, M. Sc. Thesis. Ain Shams Univ., 2008.

El-Isa, Z., Merghelani, H., Bazari, M., 1984. The Gulf of Aqaba earthquake swarm of 1983. Geophys. J. R. Astron. Soc. 76, 711–722.

Fairhead, J.D., Girdler, R.W., 1970. The seismicity of the Red Sea, Gulf of Aden, and Afar triangle. Philos. Trans. Res. Soc. London 267, 49–74.

Garfunkel, Z., 1981. Internal structure of the Dead Sea leaky transform (rift) in relation to plate kinematics. Tectonophysics 80, 81–108.

Garfunkel, Z., 2004. Origin of the Eastern Mediterranean Basin: a reevaluation. Tectonophysics 391 (1–4), 11–34.

Giermann, G., 1969. The Eastern Mediterranean ridge. Rapp. Comm. Int. Mer. Medit. 194, 605–607.

Girdler, R.W., Styles, P., 1978. Sea floor spreading in the western Gulf of Aden. Nature 271, 615–617.

Girgis, M.S., 2010. High frequency ground-motion scaling in the Northern Egypt, Ph. D Thesis. Ain Shams Univ. p. 161.

Gutenberg, B., Richter, C.F., 1944. Frequency of earthquakes in California. Bull. Seismol. Soc. Am. 34, 185–188.

Hinz, K., 1974. Results of seismic refraction and seismic reflection measurements in the Ionian Sea. Geol. J. 2, 35–65.

Hosney, A., El-Hady, S., Guideralli, M., Panza, G., 2011. Source moment tensors of the earthquake swarm in Abu Dabbab area south-east Egypt. Rend. Fis. Acc. Lincei. http://dx.doi.org/10.1007/s12210-011-0158-9.

IPRG Seismological Bulletins, 1982–1996. Earthquakes in and around Israel, Seismol. In: Division, Inst. Petrol. Res. Geophys., Holon, Israel. Available from: <http://www.gii.co.il/>.

Kijko, A., 2004. Estimation of the maximum earthquake magnitude, M_{max}. Pure Appl. Geophys. 161, 1655–1681.

Kijko, A., Graham, G., 1999. "Parametric-historic" procedure for probabilistic seismic hazard analysis—part II: assessment of seismic hazard at specified site. Pure Appl. Geophys. 154, 1–22.

Klinger, Y., Rivera, L., Haessler, H., Maurin, J.C., 1999. Active faulting in the Gulf of Aqaba: new knowledge from the MW 7.3 earthquake of 22 November 1995. Bull. Seismol. Soc. Am. 89, 1025–1036.

Le Pichon, X., Angelier, J., 1979. The Hellenic arc and trench system. A key to the neotectonics of the Eastern Mediterranean. Tectonophysics 60, 1–42.

Lort, J., Limond, W., Gray, F., 1974. Preliminary seismic studies in the Eastern Mediterranean. Earth Planet. Sci. Lett. 12, 355–366.

Maamoun, M., Allam, A., Megahed, A., 1984. Seismicity of Egypt. Bull. HIAG, 109–160.

Mackenzie, D., 1978. Active tectonics of the Alpine-Himalayan belt: the Aegean and surrounding regions. Geophys. J. R. Astron. Soc. 55, 217–254.

McKenzie, D., 1970. Plate tectonics of the Mediterranean region. Nature 326, 239–243.

McKenzie, D., 1972. Active tectonics in the Mediterranean region. Geophys. J. Res. Astron. Soc. 30, 109–185.

Meshref, W., 1990. Tectonic framework. In: Said, R. (Ed.), The Geology of Egypt. A.A. Balkema, Rotterdam, Netherlands, pp. 113–155.

Ordaz, M., Aguilar, A., Arboleda, J., 2007. CRISIS 2007. Institute of Engineering, UNAM, Mexico City, Mexico.

Papaiouannou, C. Papazachos, C., 2000. Time-independent and time-dependent seismic hazard in Greece based on seismogenic sources. Bull. Seismol. Soc. Am. 901 (1), 22–33.

Papazachos, B., Comninakis, P., 1978. Deep structure and tectonics of the Eastern Mediterranean. Tectonophysics 46, 285–296.

Poirier, J., Taher, M., 1980. Historical seismicity in the Near and Middle East, north Africa, and Spain from Arabic documents (VIIth–XVIIth century). Bull. Seismol. Soc. Am. 70, 2185–2201.

Rabinowitz, P., Ryan, W., 1970. Gravity anomalies and crustal shortening in the Eastern Mediterranean. Tectonophysics 5–6, 585–608.

Robson, D., 1971. The structure of the Gulf of Suez (Clysmic) rift with special reference to the eastern side. Q.J. Geol. Soc. London 115, 247–276.

Rotstein, Y., Kafka, A., 1982. Seismotectonics of the southern boundary of Anatolia, Eastern Mediterranean region: subduction, collision and arc jumping. J. Geophys. Res. 87, 7694–7706.

Rydelek, P.A., Sacks, I.S., 2003. Comment on ''minimum magnitude of completeness in earthquake catalogs: examples from Alaska, the western United States, and Japan'', by Stefan Wiemer and Max Wyss. Bull. Seismol. Soc. Am. 93, 1862–1867.

Salamon, A., Hofstetter, A., Garfunkel, Z., Ron, H., 1996. Seismicity of the Eastern Mediterranean region: perspective from the Sinai subplate. Tectonophysics 263, 293–305.

Salamon, A., Avraham, H., Garfunkel, Z., Ron, H., 2003. Seismotectonics of Sinai subplate-Eastern Mediterranean region. Geophys. J. Int. 155, 149–173.

Shamir, G., Shapira, A., 1994. Earthquake sequences in the Gulf of Elat. 27th General Assembly IASPEI, Wellington, New Zealand.

Stampfli, G., Borel, G., Cavazza, W., Mosar, J., Ziegler, P.A., 2001. The Paleotectonic Atlas of the PeriTethyan Domain. European Geophysical Society, CD ROM.

Stepp, J.C., 1972. Analysis of completeness of the earthquake sample in the Puget Sound area and its effect on statistical estimates of earthquake hazard. In: Proc. 2nd Int. Conf. on Microzonation, pp. 897–910.

Taymaz, T., Jackson, J., Westaway, R., 1990. Earthquake mechanism in the Hellenic trench near Crete. Geophys. J. Int. 102, 695–731.

Torlid, V.E., Hofstetter, R., 1989. Micro earthquake activity in the Dead Sea region. Geophys. J. Int. 99, 605–620.

Weichert, D.H., 1980. Estimation of the earthquakes recurrence parameters for unequal observation periods for different magnitudes. Bull. Seismol. Soc. Am. 70, 1337–1346.

Wiemer, S., Wyss, M., 2000. Minimum magnitude of complete reporting in earthquake catalogs: examples from Alaska, the Western United States, and Japan. Bull. Seismol. Soc. Am. 90, 859–869.

Wiemer, S., Wyss, M., 2003. Reply to ''Comment on 'Minimum magnitude of completeness in earthquake catalogs: examples from Alaska, the western United States, and Japan', by Stefan Wiemer andMax Wyss'', by Paul A. Rydelek and I.S. Sacks. Bull. Seismol. Soc. Am. 93, 1868–1871.

Wong, H., Zarudzki, E., Gierman, K., 1971. Some geophysical profiles in the Eastern Mediterranean. Geol. Soc. Am. Bull. 82, 91–100.

Youngs, R.R., Chiou, S.J., Silva, W., Humphrey, J.R., 1997. Strong ground motion attenuation relationships for subduction zone earthquakes. Seismo. Res. Lett. 68, 58–73.

Zhao, John X., Zhang, Jian, Asano, Akihiro, Ohno, Yuki, Oouchi, Taishi, Takahashi, Toshimasa, Ogawa, Hiroshi, Irikura, Kojiro, Thio, Hong K., Somerville, Paul G., Fukushima, Yasuhiro, Fukushima, Yoshimitsu, 2006. Attenuation relations of strong ground motion in Japan using site classification based on predominant period. Bull. Seismol. Soc. Am. 96 (3), 898–913. http://dx.doi.org/10.1785/0120050122.